East Asian Journal on Applied Mathematics
doi: 10.4208/eajam.2025-149.031125

Vol. **xx**, No. x, pp. 1-25
xxx 2025

Energy-Stable Full Discretization of the Modified Elastic Flow of Closed Curves

Cuiling Ma, Xufeng Xiao* and Xinlong Feng

College of Mathematics and Systems Science, Xinjiang University, Urumqi 830046, P.R. China.

Received 11 August 2025; Accepted (in revised version) 3 November 2025.

Abstract. An energy-stable full discretization for the modified elastic flow of closed curves is proposed. This is a gradient flow of a modified elastic energy combining bending and Dirichlet energies. The minimization of Dirichlet energy can lead to improved mesh quality. Gradient flows for both isotropic and anisotropic cases are considered. We derive new evolution equations for the parameterization and curvature vector of curves in arbitrary codimension. The proposed formulation is discretized by a parametric finite element method in space and a first-order implicit scheme in time. We establish the unconditional energy stability for the fully discretized scheme. Additionally, the second-order accuracy of the BDF2 scheme is demonstrated. Numerical examples in two and three dimensions illustrate the efficiency, energy stability, and asymptotic mesh distribution of the method for simulating the modified elastic flow.

AMS subject classifications: 65M60, 65M12, 53E40, 35G20

Key words: Curve evolution, elastic flow, parametric finite element method, unconditional stability, Dirichlet energy.

1. Introduction

The elastic energy functional is of great importance in various fields, including differential geometry, computer graphics, and mathematical modeling [10, 11, 26, 36]. Elastic flow describes the dynamic motion of a curve driven by elastic energy minimization. The equilibrium shapes associated with critical points of the elastic energy are known as elastic curves. In this paper, we present energy-stable numerical schemes for the simulation of elastic flow of closed curves with isotropic and anisotropic energies in $\mathbb{R}^n$, $n \in \mathbb{N}^+$ and $n \geq 2$.

Isotropic case. Recall that the classical isotropic elastic energy is defined by

$$E_{\tilde{\lambda}_1}(t) = E(t) + \tilde{\lambda}_1 L(t), \tag{1.1}$$

*Corresponding author. *Email addresses:* mcl1024@stu.xju.edu.cn (C.L. Ma), xiaoxufeng111@sina.com (X.F. Xiao), fxlmath@xju.edu.cn (X.L. Feng)

where $E(t)=\int_{\Gamma_t}|\boldsymbol{\kappa}|^2ds/2$ and $L(t)=\int_{\mathbb{I}}|\boldsymbol{x}_\rho|d\rho$ are respectively the bending energy and the length functional, $\tilde{\lambda}_1\geq 0$ is a constant, s denotes the arc-length of a curve Γ_t, $ds=|\boldsymbol{x}_\rho|d\rho$, $\rho\in\bar{\mathbb{I}}=[0,1]$ is a time-independent variable, and $\mathbb{I}=\mathbb{R}/\mathbb{Z}$ represents the periodic unit interval. Besides, the isotropic curvature vector $\boldsymbol{\kappa}$ is defined by

$$\boldsymbol{\kappa}=\boldsymbol{x}_{ss}, \tag{1.2}$$

and $\boldsymbol{x}(\cdot)=(x_1(\cdot),x_2(\cdot),\cdots,x_n(\cdot)):\bar{\mathbb{I}}\to\mathbb{R}^n$ denotes the parameterization of a curve. Let $\boldsymbol{\tau}=\boldsymbol{x}_s$ be the tangent vector and $\nabla_s\boldsymbol{f}:=\boldsymbol{f}_s-(\boldsymbol{f}_s\cdot\boldsymbol{\tau})\boldsymbol{\tau}$ denote the normal projection of a vector-valued function $\boldsymbol{f}$. The L^2-gradient flow of $E_{\tilde{\lambda}_1}(t)$ is given by

$$\boldsymbol{x}_t=-\nabla_s^2\boldsymbol{\kappa}-\frac{1}{2}|\boldsymbol{\kappa}|^2\boldsymbol{\kappa}+\tilde{\lambda}_1\boldsymbol{\kappa}.$$

It is called the isotropic elastic flow. Here we consider a modified isotropic elastic energy $E_{\lambda_1}(t)$ penalized by the Dirichlet energy $D(t)$ as follows:

$$E_{\lambda_1}(t)=E(t)+\lambda_1 D(t),\quad D(t):=\frac{1}{2}\int_{\mathbb{I}}|\boldsymbol{x}_\rho|^2d\rho, \tag{1.3}$$

where $\lambda_1\geq 0$ is a constant. The minimization of $D(t)$ is effective for improving the mesh quality in evolving interface problems, as shown in [17–19]. The L^2-gradient flow of the isotropic energy functional $E_{\lambda_1}(t)$ is given by

$$\boldsymbol{x}_t=-\nabla_s^2\boldsymbol{\kappa}-\frac{1}{2}|\boldsymbol{\kappa}|^2\boldsymbol{\kappa}+\lambda_1\boldsymbol{x}_{\rho s}. \tag{1.4}$$

We refer to (1.4) as the modified isotropic elastic flow. In the previous work [33], the authors illustrated that the set of stationary points of $E_{\lambda_1}(t)$ is equivalent to that of the classical isotropic elastic energy $E_{\tilde{\lambda}_1}(t)$. This observation is beneficial for analyzing error estimates and improving the mesh quality, since it allows minimizing the Dirichlet energy. Therefore, we consider the energy functional (1.3) instead of (1.1).

Anisotropic case. The classical anisotropic elastic energy $E_{\tilde{\lambda}_2}$ is defined as

$$E_{\tilde{\lambda}_2}(t)=E_\gamma(t)+\tilde{\lambda}_2 L_\gamma(t), \tag{1.5}$$

where $E_\gamma(t):=\int_{\Gamma_t}|\boldsymbol{\kappa}_\gamma|^2ds/2$ and $L_\gamma(t):=\int_{\mathbb{I}}\gamma(\boldsymbol{x}_\rho)d\rho$ are respectively the anisotropic bending energy and the weighted length functional, and $\tilde{\lambda}_2\geq 0$ is a constant. Moreover, the anisotropic function $\gamma\in C^2(\mathbb{R}^n\backslash\{\boldsymbol{0}\},\mathbb{R}^+)\cap C(\mathbb{R}^n,\mathbb{R}^+)$ is convex, and positively homogeneous of degree one — i.e.

$$\gamma(\lambda\boldsymbol{p})=\lambda\gamma(\boldsymbol{p})\quad\text{for all}\quad\boldsymbol{p}\in\mathbb{R}^n\quad\text{and all}\quad\lambda\in\mathbb{R}^+.$$

This yields

$$\gamma'(\boldsymbol{p})\cdot\boldsymbol{p}=\gamma(\boldsymbol{p}),\quad\gamma''(\boldsymbol{p})\boldsymbol{p}=\boldsymbol{0}\quad\text{for all}\quad\boldsymbol{p}\in\mathbb{R}^n\backslash\{\boldsymbol{0}\}, \tag{1.6}$$

where γ' and γ'' are respectively the gradient and the Hessian matrix of γ. The anisotropic curvature vector $\boldsymbol{\kappa}_\gamma$ is defined by

$$\boldsymbol{\kappa}_\gamma = (\gamma'(\boldsymbol{x}_s))_s. \tag{1.7}$$

The L^2-gradient flow of (1.5) has the form

$$\boldsymbol{x}_t = \big(\gamma''(\boldsymbol{x}_s)(\boldsymbol{\kappa}_\gamma)_s\big)_s - \frac{1}{2}\big(|\boldsymbol{\kappa}_\gamma|^2\boldsymbol{x}_s\big)_s + \tilde{\lambda}_2\boldsymbol{\kappa}_\gamma.$$

Similarly, we consider a modified anisotropic elastic energy E_{λ_2} defined as

$$E_{\lambda_2}(t) = E_\gamma(t) + \lambda_2 D_\gamma(t), \quad D_\gamma(t) := \frac{1}{2}\int_{\mathbb{I}} \gamma^2(\boldsymbol{x}_\rho)d\rho, \tag{1.8}$$

where $D_\gamma(t)$ is the Dirichlet energy related to the anisotropic curve, and $\lambda_2 \geq 0$ is a constant. The L^2-gradient flow of $E_{\lambda_2}(t)$ is given by

$$\boldsymbol{x}_t = -\big(\gamma''(\boldsymbol{x}_s)(\boldsymbol{\kappa}_\gamma)_s\big)_s - \frac{1}{2}\big(|\boldsymbol{\kappa}_\gamma|^2\boldsymbol{x}_s\big)_s + \lambda_2\big(\gamma(\boldsymbol{x}_\rho)\gamma'(\boldsymbol{x}_\rho)\big)_s \tag{1.9}$$

$$= -\nabla_s\big(\gamma''(\boldsymbol{x}_s)(\boldsymbol{\kappa}_\gamma)_s\big) - \frac{1}{2}|\boldsymbol{\kappa}_\gamma|^2\boldsymbol{\kappa} + \lambda_2\big[\gamma(\boldsymbol{x}_\rho)(\gamma'(\boldsymbol{x}_s))_s + (\gamma(\boldsymbol{x}_\rho))_s\gamma'(\boldsymbol{x}_s)\big], \tag{1.10}$$

where we use $\gamma'(\boldsymbol{x}_\rho) = \gamma'(\boldsymbol{x}_s)$. We call (1.10) the modified anisotropic elastic flow. Note that $E_{\tilde{\lambda}_2}$ and E_{λ_2} share the same extremal points in the following sense. On the one hand, the first three terms on the right-hand side of (1.10) are all in the normal direction. The tangential velocity of $\boldsymbol{x}$ is given by

$$\boldsymbol{x}_t \cdot \boldsymbol{\tau} = \lambda_2\big(\gamma(\boldsymbol{x}_\rho)\big)_s\gamma'(\boldsymbol{x}_s)\cdot\boldsymbol{x}_s = \lambda_2\big(\gamma(\boldsymbol{x}_\rho)\big)_s\gamma(\boldsymbol{x}_s).$$

Thus, the stationary point of E_{λ_2} along the tangential direction satisfies the identity $(\gamma(\boldsymbol{x}_\rho))_s = 0$, which implies $\gamma(\boldsymbol{x}_\rho) = c_1$ (a constant). Consequently, a stationary point of E_{λ_2} is also a stationary point of $E_{\tilde{\lambda}_2}$ for $\tilde{\lambda}_2 = c_1\lambda_2/2$. On the other hand, if $\boldsymbol{x}$ is a stationary point of $E_{\tilde{\lambda}_2}$, then we have $\gamma(\boldsymbol{x}_\rho) = c_2$ (a constant) and $\boldsymbol{x}$ is a stationary point of E_{λ_2} for $\lambda_2 = 2\tilde{\lambda}_2/c_2$.

The energy decay property is an inherent characteristic of the gradient flow problem associated with an energy functional. Therefore, it is important to investigate this property of the discrete solution. There are some numerical schemes for the solutions of elastic flow [5, 6, 15]. However, because of the high nonlinearity of the elastic energy, these approaches could only guarantee the energy stability for the spatial semi-discretization. Later, Bao and Li [4] made a breakthrough by introducing a set of geometric equations that are equivalent to the original geometric flow. This allowed them to construct an energy-stable full discretization scheme for the planar Willmore flow. In this paper, we extend the approach of Bao and Li to the modified elastic flow. Recently, Barrett *et al.* [21] proposed an energy stable discretization of the planar Willmore flow based on BGN method, which has a good mesh quality. As far as the theoretical analysis of elastic flows ia concerned, the convergence and existence results are established in [12, 20, 25, 30]. Besides, there

are various studies focused on numerical approximation of elastic flows and other related issues — cf. [1, 7, 8, 13, 14, 16, 24, 27–29, 31–35, 37] and references here.

High mesh quality is essential in numerical simulations of curve evolutions. Various methods have been proposed to improve it. The BGN method is effective for solving geometric flows with tangential movements [2, 3, 5, 6]. Mesh adaptivity is another way to improve mesh quality [9], but it is time-consuming. To obtain optimal error convergence under an asymptotic mesh distribution, an artificial tangential velocity based on the BGN method is introduced in [22]. Additionally, the DeTurck trick [19] is employed to solve the mean curvature flow by coupling it with a harmonic map heat flow, demonstrating good mesh behavior through its approximation of the conformal map. The modified harmonic heat flow based on the DeTurck trick has been analyzed in [17, 18]. This method allows for good mesh-preserving evolution in small time steps. The approach of replacing the length functional with Dirichlet energy has been developed in [33] for the elastic flow. Inspired by these works, we primarily focus on parametric finite element approximation of modified isotropic and anisotropic elastic flows of closed curves, which exhibit both energy decay properties and good mesh quality.

The current work begins by rewriting the original equations (1.4) and (1.9) by using relationships between various geometric quantities and deriving the evolution equation for the curvature vector of a curve. The energy stability is first proven in the variational formulation and then extended to semi-discrete and fully discrete schemes. For the nonlinear algebraic system, Newton's method is adopted. To verify the effectiveness, energy stability, and mesh quality of the proposed approach, we select various non-trivial curves in both $\mathbb{R}^2$ and $\mathbb{R}^3$ as initial configurations.

The rest of the manuscript is structured as follows. In Section 2, we propose novel geometric equations for the modified elastic flow with isotropic and anisotropic energies of curves in $\mathbb{R}^n$ and derive the corresponding variational formulations. In Section 3, a linear parametric finite element method is employed to approximate the weak formulation in space and analyze its energy stability. In Sections 4 and 5, the backward Euler method and the second-order BDF method are adopted to approximate the semi-discretization in the time direction. It is proven that the full discretization using the backward Euler method is unconditionally energy-stable. In Section 6, numerical experiments are performed to test the convergence rate, mesh ratio, and energy decay property of the fully discrete scheme.

2. Mathematical Models

2.1. Isotropic case

The following lemma presents an alternative evolution equation for the parameterization of a curve in $\mathbb{R}^n$ evolving under the gradient flow with the modified isotropic elastic energy.

Lemma 2.1. *For a curve in arbitrary codimension evolving under the modified isotropic elastic*

flow (1.4)*, the evolution equation of the parameterization* $\boldsymbol{x}$ *can be rewritten as*

$$\boldsymbol{x}_t = -\left(\boldsymbol{\kappa}_s - (\boldsymbol{\kappa}_s \cdot \boldsymbol{x}_s)\boldsymbol{x}_s + \frac{1}{2}|\boldsymbol{\kappa}|^2 \boldsymbol{x}_s - \lambda_1 \boldsymbol{x}_\rho\right)_s.$$

Proof. We first note that

$$\begin{aligned}(\nabla_s \boldsymbol{\kappa})_s &= \big(\boldsymbol{\kappa}_s - (\boldsymbol{\kappa}_s \cdot \boldsymbol{x}_s)\boldsymbol{x}_s\big)_s \\ &= \boldsymbol{\kappa}_{ss} - (\boldsymbol{\kappa}_{ss} \cdot \boldsymbol{x}_s + \boldsymbol{\kappa}_s \cdot \boldsymbol{x}_{ss})\boldsymbol{x}_s - (\boldsymbol{\kappa}_s \cdot \boldsymbol{x}_s)\boldsymbol{x}_{ss} \\ &= \boldsymbol{\kappa}_{ss} - (\boldsymbol{\kappa}_{ss} \cdot \boldsymbol{x}_s)\boldsymbol{x}_s - (\boldsymbol{\kappa}_s \cdot \boldsymbol{\kappa})\boldsymbol{x}_s - (\boldsymbol{\kappa}_s \cdot \boldsymbol{x}_s)\boldsymbol{\kappa},\end{aligned}$$

where the last equality used the definition of $\boldsymbol{\kappa}$ in (1.2). Then we obtain

$$\nabla_s^2 \boldsymbol{\kappa} = (\nabla_s \boldsymbol{\kappa})_s - \big((\nabla_s \boldsymbol{\kappa})_s \cdot \boldsymbol{x}_s\big)\boldsymbol{x}_s = \big(\boldsymbol{\kappa}_s - (\boldsymbol{\kappa}_s \cdot \boldsymbol{x}_s)\boldsymbol{x}_s\big)_s + (\boldsymbol{\kappa}_s \cdot \boldsymbol{\kappa})\boldsymbol{x}_s, \tag{2.1}$$

where we have used the facts $|\boldsymbol{x}_s| = 1$ and $\boldsymbol{\kappa} \cdot \boldsymbol{x}_s = (|\boldsymbol{x}_s|^2)_s/2 = 0$. Finally, submitting (2.1) into (1.4) yields

$$\begin{aligned}\boldsymbol{x}_t &= -\big(\boldsymbol{\kappa}_s - (\boldsymbol{\kappa}_s \cdot \boldsymbol{x}_s)\boldsymbol{x}_s\big)_s - (\boldsymbol{\kappa}_s \cdot \boldsymbol{\kappa})\boldsymbol{x}_s - \frac{1}{2}\big(|\boldsymbol{\kappa}|^2 \boldsymbol{x}_s\big)_s + (\boldsymbol{\kappa}_s \cdot \boldsymbol{\kappa})\boldsymbol{x}_s + \lambda_1 \boldsymbol{x}_{\rho s} \\ &= -\left(\boldsymbol{\kappa}_s - (\boldsymbol{\kappa}_s \cdot \boldsymbol{x}_s)\boldsymbol{x}_s + \frac{1}{2}|\boldsymbol{\kappa}|^2 \boldsymbol{x}_s - \lambda_1 \boldsymbol{x}_\rho\right)_s,\end{aligned}$$

and the proof is complete. □

The following lemma presents an evolution equation for the curvature vector, which holds for all geometric flows of curves in $\mathbb{R}^n$.

Lemma 2.2. *For the curvature vector* $\boldsymbol{\kappa}$ *of a curve in arbitrary codimension, it satisfies the following evolution equation:*

$$\boldsymbol{\kappa}_t = \big(\boldsymbol{x}_{ts} - (\boldsymbol{x}_s \cdot \boldsymbol{x}_{ts})\boldsymbol{x}_s\big)_s - (\boldsymbol{x}_s \cdot \boldsymbol{x}_{ts})\boldsymbol{\kappa}.$$

Proof. Taking the time derivative of $\boldsymbol{\kappa}$ in (1.2) yields

$$\boldsymbol{\kappa}_t = (\boldsymbol{x}_{ss})_t = \boldsymbol{x}_{sts} - (\boldsymbol{x}_s \cdot \boldsymbol{x}_{ts})\boldsymbol{\kappa} = \big(\boldsymbol{x}_{ts} - (\boldsymbol{x}_s \cdot \boldsymbol{x}_{ts})\boldsymbol{x}_s\big)_s - (\boldsymbol{x}_s \cdot \boldsymbol{x}_{ts})\boldsymbol{\kappa},$$

where we twice used the identity $(\cdot)_{st} = (\cdot)_{ts} - (\boldsymbol{x}_s \cdot \boldsymbol{x}_{ts})(\cdot)_s$, cf., e.g. [4]. □

Thus, for the modified isotropic elastic flow, we consider the following coupled system:

$$\boldsymbol{x}_t = -\left(\boldsymbol{\kappa}_s - (\boldsymbol{\kappa}_s \cdot \boldsymbol{x}_s)\boldsymbol{x}_s + \frac{1}{2}|\boldsymbol{\kappa}|^2 \boldsymbol{x}_s - \lambda_1 \boldsymbol{x}_\rho\right)_s, \tag{2.2}$$

$$\boldsymbol{\kappa}_t = \big(\boldsymbol{x}_{ts} - (\boldsymbol{x}_s \cdot \boldsymbol{x}_{ts})\boldsymbol{x}_s\big)_s - (\boldsymbol{x}_s \cdot \boldsymbol{x}_{ts})\boldsymbol{\kappa} \tag{2.3}$$

in $\mathbb{I} \times (0, T]$, together with the initial data

$$\boldsymbol{x}(0) = \boldsymbol{x}_0, \quad \boldsymbol{\kappa}(0) = \boldsymbol{\kappa}_0 \quad \text{in } \bar{\mathbb{I}}.$$

2.2. Anisotropic case

Here, we introduce an evolution equation of the anisotropic curvature vector of curves, which is an extension of the isotropic case.

Lemma 2.3. *The anisotropic curvature vector $\boldsymbol{\kappa}_\gamma$ of a curve in arbitrary codimension satisfies the following evolution equation:*

$$(\boldsymbol{\kappa}_\gamma)_t = \big(\gamma''(\boldsymbol{x}_s)\boldsymbol{x}_{ts}\big)_s - (\boldsymbol{x}_s \cdot \boldsymbol{x}_{ts})\boldsymbol{\kappa}_\gamma.$$

Proof. Taking the time derivative of $\boldsymbol{\kappa}_\gamma$ defined in (1.7) yields

$$\begin{aligned}
(\boldsymbol{\kappa}_\gamma)_t &= \big(\gamma'(\boldsymbol{x}_s)\big)_{st} \\
&= \big(\gamma'(\boldsymbol{x}_s)\big)_{ts} - (\boldsymbol{x}_s \cdot \boldsymbol{x}_{ts})\big(\gamma'(\boldsymbol{x}_s)\big)_s \\
&= \big(\gamma''(\boldsymbol{x}_s)\boldsymbol{x}_{st}\big)_s - (\boldsymbol{x}_s \cdot \boldsymbol{x}_{ts})\boldsymbol{\kappa}_\gamma \\
&= \big(\gamma''(\boldsymbol{x}_s)\big(\boldsymbol{x}_{ts} - (\boldsymbol{x}_s \cdot \boldsymbol{x}_{ts})\boldsymbol{x}_s\big)\big)_s - (\boldsymbol{x}_s \cdot \boldsymbol{x}_{ts})\boldsymbol{\kappa}_\gamma \\
&= \big(\gamma''(\boldsymbol{x}_s)\boldsymbol{x}_{ts}\big)_s - (\boldsymbol{x}_s \cdot \boldsymbol{x}_{ts})\boldsymbol{\kappa}_\gamma,
\end{aligned}$$

where we have used the identity $\gamma''(\boldsymbol{x}_s)\boldsymbol{x}_s = \boldsymbol{0}$ from (1.6) and the identity $(\cdot)_{st} = (\cdot)_{ts} - (\boldsymbol{x}_s \cdot \boldsymbol{x}_{ts})(\cdot)_s$ from [4]. □

Thus, for the modified anisotropic elastic flow, we consider the following coupled system:

$$\boldsymbol{x}_t = -\left(\gamma''(\boldsymbol{x}_s)(\boldsymbol{\kappa}_\gamma)_s + \frac{1}{2}|\boldsymbol{\kappa}_\gamma|^2\boldsymbol{x}_s - \lambda_2\gamma(\boldsymbol{x}_\rho)\gamma'(\boldsymbol{x}_\rho)\right)_s, \tag{2.4}$$

$$(\boldsymbol{\kappa}_\gamma)_t = \big(\gamma''(\boldsymbol{x}_s)\boldsymbol{x}_{ts}\big)_s - (\boldsymbol{x}_s \cdot \boldsymbol{x}_{ts})\boldsymbol{\kappa}_\gamma \tag{2.5}$$

in $\mathbb{I} \times (0, T]$, along with the initial data

$$\boldsymbol{x}(0) = \boldsymbol{x}_0, \quad \boldsymbol{\kappa}_\gamma(0) = \boldsymbol{\kappa}_{\gamma_0} \quad \text{in } \bar{\mathbb{I}}.$$

We note that for $\gamma(\boldsymbol{p}) = |\boldsymbol{p}|$ the Eqs. (2.4)-(2.5) reduce to (2.2)-(2.3). Hence, the isotropic problem is a special case of the anisotropic problem.

3. Weak Formulation and Energy Stability

In order to derive the weak formulations for the modified isotropic elastic flow (2.2)-(2.3) and the modified anisotropic elastic flow (2.4)-(2.5), we introduce the function space

$$L^2(\Gamma_t) = \left\{\mu : \Gamma_t \to \mathbb{R} \;\middle|\; \int_{\Gamma_t} |\mu|^2 ds < +\infty\right\},$$

and the L^2-inner product

$$(\mu, \psi)_{\Gamma_t} = \int_{\Gamma_t} \mu(s)\psi(s)ds, \quad \mu, \psi \in L^2(\Gamma_t).$$

Then the Sobolev space $H^1(\Gamma_t)$ is defined by

$$H^1(\Gamma_t) = \left\{\mu : \Gamma_t \to \mathbb{R} \;\middle|\; \mu \in L^2(\Gamma_t),\ \mu_s \in L^2(\Gamma_t)\right\}.$$

3.1. Isotropic case

Following the above definitions, we respectively multiply the identities (2.2) and (2.3) by the test functions $\boldsymbol{\eta} \in [H^1(\Gamma_t)]^n$ and $\boldsymbol{\xi} \in [H^1(\Gamma_t)]^n$ and integrate by parts, thus obtaining the following weak formulation: Given initial data $(\boldsymbol{x}_0, \boldsymbol{\kappa}_0) \in [H^1(\Gamma_t)]^n \times [H^1(\Gamma_t)]^n$, find the weak solution $(\boldsymbol{x}(t), \boldsymbol{\kappa}(t)) \in [H^1(\Gamma_t)]^n \times [H^1(\Gamma_t)]^n$ such that

$$(\boldsymbol{x}_t, \boldsymbol{\eta})_{\Gamma_t} = \left(\boldsymbol{\kappa}_s - (\boldsymbol{\kappa}_s \cdot \boldsymbol{x}_s)\boldsymbol{x}_s + \frac{1}{2}|\boldsymbol{\kappa}|^2 \boldsymbol{x}_s - \lambda_1 \boldsymbol{x}_\rho, \boldsymbol{\eta}_s \right)_{\Gamma_t}, \tag{3.1}$$

$$\left(\boldsymbol{\kappa}_t, \boldsymbol{\xi}\right)_{\Gamma_t} = -\left(\boldsymbol{x}_{ts} - (\boldsymbol{x}_s \cdot \boldsymbol{x}_{ts})\boldsymbol{x}_s, \boldsymbol{\xi}_s\right)_{\Gamma_t} - \left((\boldsymbol{x}_s \cdot \boldsymbol{x}_{ts})\boldsymbol{\kappa}, \boldsymbol{\xi}\right)_{\Gamma_t} \tag{3.2}$$

for $t \in (0, T]$. Then the following energy-stable property for the modified isotropic elastic flow is available.

Theorem 3.1. *For $(\boldsymbol{x}(t), \boldsymbol{\kappa}(t)) \in [H^1(\Gamma_t)]^n \times [H^1(\Gamma_t)]^n$ with the initial curve Γ_0, the weak formulation* (3.1)-(3.2) *has the energy-decay property*

$$E_{\lambda_1}(t) \le E_{\lambda_1}(\tilde{t}) \le E_{\lambda_1}(0) = \frac{1}{2}\int_{\Gamma_0} |\boldsymbol{\kappa}_0|^2 ds + \frac{\lambda_1}{2}\int_{\mathbb{I}} |(\boldsymbol{x}_0)_\rho|^2 d\rho \quad \textit{for all} \quad t \ge \tilde{t} > 0.$$

Proof. The proof is analogous and simple to the argument in the anisotropic case, i.e., Theorem 3.2. □

3.2. Anisotropic case

Similar to isotropic case, we obtain weak formulation for the modified anisotropic elastic flow (2.4)-(2.5): Given initial data $(\boldsymbol{x}_0, \boldsymbol{\kappa}_{\gamma_0}) \in [H^1(\Gamma_t)]^n \times [H^1(\Gamma_t)]^n$, find $(\boldsymbol{x}(t), \boldsymbol{\kappa}_\gamma(t)) \in [H^1(\Gamma_t)]^n \times [H^1(\Gamma_t)]^n$ such that

$$(\boldsymbol{x}_t, \boldsymbol{\eta})_{\Gamma_t} = \left(\gamma''(\boldsymbol{x}_s)(\boldsymbol{\kappa}_\gamma)_s + \frac{1}{2}|\boldsymbol{\kappa}_\gamma|^2 \boldsymbol{x}_s - \lambda_2 \gamma(\boldsymbol{x}_\rho)\gamma'(\boldsymbol{x}_\rho), \boldsymbol{\eta}_s \right)_{\Gamma_t}, \tag{3.3}$$

$$\left((\boldsymbol{\kappa}_\gamma)_t, \boldsymbol{\xi}\right)_{\Gamma_t} = -\left(\gamma''(\boldsymbol{x}_s)\boldsymbol{x}_{ts}, \boldsymbol{\xi}_s\right)_{\Gamma_t} - \left((\boldsymbol{x}_s \cdot \boldsymbol{x}_{ts})\boldsymbol{\kappa}_\gamma, \boldsymbol{\xi}\right)_{\Gamma_t} \tag{3.4}$$

for all $(\boldsymbol{\eta}, \boldsymbol{\xi}) \in [H^1(\Gamma_t)]^n \times [H^1(\Gamma_t)]^n$ and $t \in (0, T]$.

Then the following energy-stable property for the modified anisotropic elastic flow is available.

Theorem 3.2. *For $(\boldsymbol{x}(t), \boldsymbol{\kappa}_\gamma(t)) \in [H^1(\Gamma_t)]^n \times [H^1(\Gamma_t)]^n$ with the initial curve Γ_0, the weak formulation* (3.3)-(3.4) *has the energy-decay property*

$$E_{\lambda_2}(t) \le E_{\lambda_2}(\tilde{t}) \le E_{\lambda_2}(0) = \frac{1}{2}\int_{\Gamma_0} |\boldsymbol{\kappa}_{\gamma_0}|^2 ds + \frac{\lambda_2}{2}\int_{\mathbb{I}} \gamma^2\big((\boldsymbol{x}_0)_\rho\big) d\rho \quad \textit{for all} \quad t \ge \tilde{t} > 0. \tag{3.5}$$

Proof. Taking the time derivative of $E_{\lambda_2}(t)$ yields

$$\begin{aligned}\frac{d}{dt}E_{\lambda_2}(t) &= \frac{1}{2}\frac{d}{dt}\int_{\Gamma_t}|\boldsymbol{\kappa}_\gamma|^2 ds + \frac{\lambda_2}{2}\frac{d}{dt}\int_{\mathbb{I}}\gamma^2(\boldsymbol{x}_\rho)d\rho \\ &= \big((\boldsymbol{\kappa}_\gamma)_t, \boldsymbol{\kappa}_\gamma\big)_{\Gamma_t} + \frac{1}{2}\big(|\boldsymbol{\kappa}_\gamma|^2\boldsymbol{x}_s, \boldsymbol{x}_{ts}\big)_{\Gamma_t} + \lambda_2\big(\gamma(\boldsymbol{x}_\rho)\gamma'(\boldsymbol{x}_\rho), \boldsymbol{x}_{ts}\big)_{\Gamma_t},\end{aligned}$$

where we have used the identities $\boldsymbol{x}_{\rho t} = |\boldsymbol{x}_\rho|\boldsymbol{x}_{ts}$ and $|\boldsymbol{x}_\rho|_t = |\boldsymbol{x}_\rho|\boldsymbol{x}_s \cdot \boldsymbol{x}_{ts}$. Let $\boldsymbol{\eta} = \boldsymbol{x}_t$ and $\boldsymbol{\xi} = \boldsymbol{\kappa}_\gamma$ in (3.3) and (3.4), respectively, we obtain

$$\big(\boldsymbol{x}_t, \boldsymbol{x}_t\big)_{\Gamma_t} + \big((\boldsymbol{\kappa}_\gamma)_t, \boldsymbol{\kappa}_\gamma\big)_{\Gamma_t} = -\frac{1}{2}\big(|\boldsymbol{\kappa}_\gamma|^2\boldsymbol{x}_s, \boldsymbol{x}_{ts}\big)_{\Gamma_t} - \lambda_2\big(\gamma(\boldsymbol{x}_\rho)\gamma'(\boldsymbol{x}_\rho), \boldsymbol{x}_{ts}\big)_{\Gamma_t}.$$

Then we deduce that

$$\frac{d}{dt}E_{\lambda_2}(t) = -(\boldsymbol{x}_t, \boldsymbol{x}_t)_{\Gamma_t} \le 0,$$

which immediately implies (3.5). □

4. Spatial Semi-Discretized Scheme and Energy Stability

In this section, we discretize the weak formulations of isotropic elastic flow (3.1)-(3.2) and anisotropic elastic flow (3.3)-(3.4) in spatial direction, and establish the energy stability of the corresponding semi-discretizations. We divide the reference interval $\mathbb{I}$ into a set of uniform partitions: $[0,1] = \cup_{j=1}^J I_j = \cup_{j=1}^J [\rho_{j-1}, \rho_j]$, $J \ge 3$, with nodes $\rho_j = jh$, $j = 0, \ldots, J$ and $h = J^{-1}$. The linear finite element space $\mathbb{V}^h$ with the periodic boundary condition is defined by

$$\mathbb{V}^h := \Big\{\mu^h \in C(\bar{\mathbb{I}}) \;\Big|\; \mu^h|_{I_j} \in P_1(I_j),\ \ j = 1, \ldots, J,\ \ \mu^h(\rho_0) = \mu^h(\rho_J)\Big\},$$

where $P_1(I_j)$ refers to the set of all polynomials on I_j of the degree at most 1. Let $\boldsymbol{x}^h(\mathbb{I}, t) = (x_1^h(\mathbb{I}, t), x_2^h(\mathbb{I}, t), \cdots, x_n^h(\mathbb{I}, t))^T \in [\mathbb{V}^h]^n$ be an approximation of the parameterization $\boldsymbol{x}(t)$ and $\{\boldsymbol{h}_j\}_{j=1}^J$ the ordered line segments

$$\boldsymbol{h}_j := \boldsymbol{x}^h(\rho_j) - \boldsymbol{x}^h(\rho_{j-1}).$$

Consequently, the approximation $\Gamma^h := \bigcup_{j=1}^J \boldsymbol{h}_j$ is a polygonal curve. We also assume that $|\boldsymbol{x}_\rho^h(\cdot, t)| > 0$, $t \in (0, T]$ and define the discretized arc length derivative by

$$\omega_s^h|_{I_j} := \frac{\omega_\rho^h}{|\boldsymbol{x}_\rho^h|}\bigg|_{I_j} = \frac{\omega^h(\rho_j) - \omega^h(\rho_{j-1})}{|\boldsymbol{h}_j|}, \quad j = 1, \ldots, J, \tag{4.1}$$

this definition can be naturally extended to vector-valued functions.

In addition, to simplify the calculations in the energy decay proof and maintain second-order numerical accuracy, we introduce the following mass-lumped L^2-inner product

$$\left(\xi^h, \boldsymbol{\mu}^h\right)_{\Gamma^h} = \frac{1}{2}\sum_{j=1}^{J} |\boldsymbol{h}_j| \Big[(\xi^h \cdot \boldsymbol{\mu}^h)(\rho_j^-) + (\xi^h \cdot \boldsymbol{\mu}^h)(\rho_{j-1}^+) \Big] \tag{4.2}$$

for ξ^h, $\boldsymbol{\mu}^h \in [\mathbb{V}^h]^n$, with possible jumps at the points ρ_j, where $\boldsymbol{f}(\rho_j^{\pm}) = \lim_{\epsilon\to 0} \boldsymbol{f}(\rho_j \pm \epsilon)$, $j = 0, \ldots, J$.

4.1. Isotropic case

From the above introduction, we can obtain the following semi-discretized formulation: Given initial data $(\boldsymbol{x}_0, \boldsymbol{\kappa}_0) \in [\mathbb{V}^h]^n \times [\mathbb{V}^h]^n$, find discrete solution $(\boldsymbol{x}^h(t), \boldsymbol{\kappa}^h(t)) \in [\mathbb{V}^h]^n \times [\mathbb{V}^h]^n$ such that

$$\left(\boldsymbol{x}_t^h, \boldsymbol{\eta}^h\right)_{\Gamma_t^h} = \left(\boldsymbol{\kappa}_s^h - (\boldsymbol{\kappa}_s^h \cdot \boldsymbol{x}_s^h)\boldsymbol{x}_s^h + \frac{1}{2}|\boldsymbol{\kappa}^h|^2 \boldsymbol{x}_s^h - \lambda_1 \boldsymbol{x}_\rho^h, \boldsymbol{\eta}_s^h \right)_{\Gamma_t^h}, \tag{4.3}$$

$$\left(\boldsymbol{\kappa}_t^h, \xi^h\right)_{\Gamma_t^h} = -\left(\boldsymbol{x}_{ts}^h - (\boldsymbol{x}_s^h \cdot \boldsymbol{x}_{ts}^h)\boldsymbol{x}_s^h, \xi_s^h\right)_{\Gamma_t^h} - \left((\boldsymbol{x}_s^h \cdot \boldsymbol{x}_{ts}^h)\boldsymbol{\kappa}^h, \xi^h\right)_{\Gamma_t^h} \tag{4.4}$$

for all $(\boldsymbol{\eta}^h,\ \xi^h) \in [\mathbb{V}^h]^n \times [\mathbb{V}^h]^n$ and $t \in (0, T]$, where $\Gamma_t^h = \Gamma^h(t)$.

Recalling the definition of the modified isotropic elastic energy in (1.3) and discretized inner product in (4.2), the semi-discretized energy functional is naturally defined as

$$\begin{aligned} E_{\lambda_1}^h(t) &= E^h(t) + \lambda_1 D^h(t) \\ &= \frac{1}{2}\left(\boldsymbol{\kappa}^h, \boldsymbol{\kappa}^h\right)_{\Gamma_t^h} + \frac{\lambda_1}{2}\left(\boldsymbol{x}_\rho^h, \boldsymbol{x}_\rho^h\right)_{\mathbb{I}} \\ &= \frac{1}{4}\sum_{j=1}^{J} |\boldsymbol{h}_j| \Big[|\boldsymbol{\kappa}^h(\rho_j^-)|^2 + |\boldsymbol{\kappa}^h(\rho_{j-1}^+)|^2 \Big] + \frac{\lambda_1}{2h}\sum_{j=1}^{J} |\boldsymbol{h}_j|^2, \end{aligned}$$

then we can derive the energy stability of the semi-discretized scheme as follows:

Theorem 4.1. *For $(\boldsymbol{x}^h(t), \boldsymbol{\kappa}^h(t)) \in [\mathbb{V}^h]^n \times [\mathbb{V}^h]^n$ with the initial discrete curve Γ_0^h, and $t \geq \tilde{t} > 0$, the semi-discretization* (4.3)-(4.4) *has the energy-decay property*

$$E_{\lambda_1}^h(t) \leq E_{\lambda_1}^h(\tilde{t}) \leq E_{\lambda_1}^h(0) = \frac{1}{4}\sum_{j=1}^{J} |\boldsymbol{h}_{0_j}| \Big[|\boldsymbol{\kappa}_0^h(\rho_j^-)|^2 + |\boldsymbol{\kappa}_0^h(\rho_{j-1}^+)|^2 \Big] + \frac{\lambda_1}{2h}\sum_{j=1}^{J} |\boldsymbol{h}_{0_j}|^2.$$

Proof. It is similar to the proof of Theorem 4.2 below. □

4.2. Anisotropic case

For the modified anisotropic elastic flow (3.3)-(3.4), we can obtain the following semi-discretized formulation: Given initial data $(\boldsymbol{x}_0, \boldsymbol{\kappa}_{\gamma_0}) \in [\mathbb{V}^h]^n \times [\mathbb{V}^h]^n$, find discrete solution $(\boldsymbol{x}^h(t), \boldsymbol{\kappa}^h_\gamma(t)) \in [\mathbb{V}^h]^n \times [\mathbb{V}^h]^n$ such that

$$\left(\boldsymbol{x}^h_t, \boldsymbol{\eta}^h\right)_{\Gamma^h_t} = \left(\gamma''(\boldsymbol{x}^h_s)(\boldsymbol{\kappa}^h_\gamma)_s + \frac{1}{2}|\boldsymbol{\kappa}^h_\gamma|^2 \boldsymbol{x}^h_s - \lambda_2 \gamma(\boldsymbol{x}^h_\rho)\gamma'(\boldsymbol{x}^h_\rho), \boldsymbol{\eta}^h_s\right)_{\Gamma^h_t}, \tag{4.5}$$

$$\left((\boldsymbol{\kappa}^h_\gamma)_t, \boldsymbol{\xi}^h\right)_{\Gamma^h_t} = -\left(\gamma''(\boldsymbol{x}^h_s)\boldsymbol{x}^h_{ts}, \boldsymbol{\xi}^h_s\right)_{\Gamma^h_t} - \left((\boldsymbol{x}^h_s \cdot \boldsymbol{x}^h_{ts})\boldsymbol{\kappa}^h_\gamma, \boldsymbol{\xi}^h\right)_{\Gamma^h_t} \tag{4.6}$$

for all $(\boldsymbol{\eta}^h,\ \boldsymbol{\xi}^h) \in [\mathbb{V}^h]^n \times [\mathbb{V}^h]^n$ and $t \in (0, T]$.

The discretization of the modified anisotropic elastic energy in (1.8) has the form

$$\begin{aligned} E^h_{\lambda_2}(t) &= E^h_\gamma(t) + \lambda_2 D^h_\gamma(t) \\ &= \frac{1}{2}\left(\boldsymbol{\kappa}^h_\gamma, \boldsymbol{\kappa}^h_\gamma\right)_{\Gamma^h_t} + \frac{\lambda_2}{2}\left(\gamma(\boldsymbol{x}^h_\rho), \gamma(\boldsymbol{x}^h_\rho)\right)_{\mathbb{I}} \\ &= \frac{1}{4}\sum_{j=1}^{J} |\boldsymbol{h}_j| \left[\left|\boldsymbol{\kappa}^h_\gamma(\rho^-_j)\right|^2 + \left|\boldsymbol{\kappa}^h_\gamma(\rho^+_{j-1})\right|^2\right] \\ &\quad + \frac{\lambda_2 h}{4}\sum_{j=1}^{J}\left[\gamma^2\left(\boldsymbol{x}^h_\rho(\rho^-_j)\right) + \gamma^2\left(\boldsymbol{x}^h_\rho(\rho^+_{j-1})\right)\right]. \end{aligned} \tag{4.7}$$

The following theorem describes the energy stability of the semi-discretized scheme.

Theorem 4.2. *For $(\boldsymbol{x}^h(t), \boldsymbol{\kappa}^h_\gamma(t)) \in [\mathbb{V}^h]^n \times [\mathbb{V}^h]^n$ with an initial discrete curve Γ^h_0, the semi-discretization* (4.5)-(4.6) *has the energy-decay property*

$$\begin{aligned} &E^h_{\lambda_2}(t) \le E^h_{\lambda_2}(\tilde{t}) \le E^h_{\lambda_2}(0) \\ &= \frac{1}{4}\sum_{j=1}^{J} |\boldsymbol{h}_{0_j}| \left[\left|\boldsymbol{\kappa}^h_{\gamma_0}(\rho^-_j)\right|^2 + \left|\boldsymbol{\kappa}^h_{\gamma_0}(\rho^+_{j-1})\right|^2\right] \\ &\quad + \frac{\lambda_2 h}{4}\sum_{j=1}^{J}\left[\gamma^2\left(\boldsymbol{x}^h_\rho(\rho^-_j)\right) + \gamma^2\left(\boldsymbol{x}^h_\rho(\rho^+_{j-1})\right)\right] \end{aligned} \tag{4.8}$$

for all $t \ge \tilde{t} > 0$.

Proof. The time derivative of the semi-discretized energy $E^h_{\lambda_2}(t)$ in (4.7) is

$$\begin{aligned} \frac{d}{dt}E^h_{\lambda_2}(t) &= \frac{1}{4}\sum_{j=1}^{J} |\boldsymbol{h}_j| \left(\boldsymbol{x}^h_s \cdot \boldsymbol{x}^h_{ts}\right)\Big|_{I_j} \left[\left|\boldsymbol{\kappa}^h_\gamma(\rho^-_j)\right|^2 + \left|\boldsymbol{\kappa}^h_\gamma(\rho^+_{j-1})\right|^2\right] \\ &\quad + \frac{1}{2}\sum_{j=1}^{J} |\boldsymbol{h}_j| \left[\left((\boldsymbol{\kappa}^h_\gamma)_t \cdot \boldsymbol{\kappa}^h_\gamma\right)(\rho^-_j) + \left((\boldsymbol{\kappa}^h_\gamma)_t \cdot \boldsymbol{\kappa}^h_\gamma\right)(\rho^+_{j-1})\right] \end{aligned}$$

$$+\frac{\lambda_2 h}{2}\sum_{j=1}^{J}\Big[\gamma\big(\boldsymbol{x}_\rho^h(\rho_j^-)\big)\gamma_t\big(\boldsymbol{x}_\rho^h(\rho_j^-)\big)+\gamma\big(\boldsymbol{x}_\rho^h(\rho_{j-1}^+)\big)\gamma_t\big(\boldsymbol{x}_\rho^h(\rho_{j-1}^+)\big)\Big]$$
$$=\frac{1}{2}\Big(|\boldsymbol{\kappa}_\gamma^h|^2\boldsymbol{x}_s^h,\boldsymbol{x}_{ts}^h\Big)_{\Gamma_t^h}+\Big((\boldsymbol{\kappa}_\gamma^h)_t,\boldsymbol{\kappa}_\gamma^h\Big)_{\Gamma_t^h}+\lambda_2\Big(\gamma(\boldsymbol{x}_\rho^h)\gamma'(\boldsymbol{x}_\rho^h),\boldsymbol{x}_{ts}^h\Big)_{\Gamma_t^h},$$

where we have used the identity — cf. [4, Eq. (3.9)],

$$|\boldsymbol{h}_j|_t=|\boldsymbol{h}_j|\big(\boldsymbol{x}_s^h\cdot\boldsymbol{x}_{ts}^h\big)\big|_{I_j}=h\Big(\boldsymbol{x}_\rho^h\cdot\boldsymbol{x}_{ts}^h\Big)\big|_{I_j}.$$

Choose $\boldsymbol{\eta}^h=\boldsymbol{x}_t^h$ and $\boldsymbol{\xi}^h=\boldsymbol{\kappa}_\gamma^h$ in (4.5)-(4.6). Combining these equations yields

$$\Big(\boldsymbol{x}_t^h,\boldsymbol{x}_t^h\Big)_{\Gamma_t^h}+\Big((\boldsymbol{\kappa}_\gamma^h)_t,\boldsymbol{\kappa}_\gamma^h\Big)_{\Gamma_t^h}=-\frac{1}{2}\Big(|\boldsymbol{\kappa}_\gamma^h|^2\boldsymbol{x}_s^h,\boldsymbol{x}_{ts}^h\Big)_{\Gamma_t^h}-\lambda_2\Big(\gamma(\boldsymbol{x}_\rho^h)\gamma'(\boldsymbol{x}_\rho^h),\boldsymbol{x}_{ts}^h\Big)_{\Gamma_t^h},$$

so that

$$\frac{d}{dt}E_{\lambda_2}^h(t)=-\Big(\boldsymbol{x}_t^h,\boldsymbol{x}_t^h\Big)_{\Gamma_t^h}\le 0,$$

which implies (4.8). □

5. Fully Discretized Scheme and Energy Stability

Now we approximate the semi-discretized formulations (4.3)-(4.4) and (4.5)-(4.6) in the time direction. Let $\tau=T/N$ be the uniform time step size for a positive integer N, and denote $t_m=m\tau$, $m=1,\dots,N$ by the discrete time levels. Let $(\boldsymbol{x}^m,\boldsymbol{\kappa}^m)\in[\mathbb{V}^h]^n\times[\mathbb{V}^h]^n$ as be numerical approximation of the semi-discrete function $(\boldsymbol{x}^h(t_m),\boldsymbol{\kappa}^h(t_m))\in[\mathbb{V}^h]^n\times[\mathbb{V}^h]^n$. We assume that $|\boldsymbol{x}_\rho^m|>0$, $m=1,\dots,N$. The ordered line segments $\boldsymbol{h}_j^m$, $j=1,\dots,J$ are defined as

$$\boldsymbol{h}_j^m:=\boldsymbol{x}^m(\rho_j)-\boldsymbol{x}^m(\rho_{j-1}).$$

Then $\Gamma^m:=\bigcup_{j=1}^J\boldsymbol{h}_j^m$ is a polygonal curve and the corresponding partial derivative is defined similar to (4.1).

5.1. Isotropic case

For the semi-discretization (4.3)-(4.4), we adopt the backward Euler method in the time direction and derive the following full discretization: Given initial approximations $(\boldsymbol{x}^0,\boldsymbol{\kappa}^0)\in[\mathbb{V}^h]^n\times[\mathbb{V}^h]^n$, find a discrete solution $(\boldsymbol{x}^m,\boldsymbol{\kappa}^m)\in[\mathbb{V}^h]^n\times[\mathbb{V}^h]^n$ such that

$$\Big(\frac{1}{\tau}\delta\boldsymbol{x}^m,\boldsymbol{\eta}^h\Big)_{\Gamma^{m-1}}=\Big(\boldsymbol{\kappa}_s^m-(\boldsymbol{\kappa}_s^m\cdot\boldsymbol{x}_s^{m-1})\boldsymbol{x}_s^{m-1}+\frac{1}{2}|\boldsymbol{\kappa}^m|^2\boldsymbol{x}_s^m-\lambda_1\boldsymbol{x}_\rho^m,\boldsymbol{\eta}_s^h\Big)_{\Gamma^{m-1}},\tag{5.1}$$

$$\big(\delta\boldsymbol{\kappa}^m,\xi^h\big)_{\Gamma^{m-1}}=-\big(\delta\boldsymbol{x}_s^m-(\boldsymbol{x}_s^{m-1}\cdot\delta\boldsymbol{x}_s^m)\boldsymbol{x}_s^{m-1},\xi_s^h\big)_{\Gamma^{m-1}}-\Big((\boldsymbol{x}_s^m\cdot\delta\boldsymbol{x}_s^m)\boldsymbol{\kappa}^m,\xi^h\Big)_{\Gamma^{m-1}}\tag{5.2}$$

for all $(\boldsymbol{\eta}^h, \boldsymbol{\xi}^h) \in [\mathbb{V}^h]^n \times [\mathbb{V}^h]^n$ and $m > 0$, where $\delta \boldsymbol{x}^m := \boldsymbol{x}^m - \boldsymbol{x}^{m-1}$ and $\delta \boldsymbol{\kappa}^m := \boldsymbol{\kappa}^m - \boldsymbol{\kappa}^{m-1}$. For simplicity, we use the following mass-lumped L^2-inner product [16]:

$$\left(\boldsymbol{\xi}^h, \boldsymbol{\mu}^h\right)_{\Gamma^m} = \frac{1}{2} \sum_{j=1}^{J} |\boldsymbol{h}_j^m| \Big[(\boldsymbol{\xi}^h \cdot \boldsymbol{\mu}^h)(\rho_j^-) + (\boldsymbol{\xi}^h \cdot \boldsymbol{\mu}^h)(\rho_{j-1}^+) \Big].$$

Let $E_{\lambda_1}^m = E^m + \lambda_1 D^m$ be the discretized energy functional. Then the unconditional energy stability is established in the following theorem.

Theorem 5.1 (Energy Decay). *For $(\boldsymbol{x}^m, \boldsymbol{\kappa}^m) \in [\mathbb{V}^h]^n \times [\mathbb{V}^h]^n$ with the initial curve Γ_0^h, the fully discretized problem* (5.1)-(5.2) *has the property*

$$\begin{aligned} & E_{\lambda_1}^m \le E_{\lambda_1}^{m-1} \le \cdots \le E_{\lambda_1}^0 \\ &= \frac{1}{4} \sum_{j=1}^{J} |\boldsymbol{h}_j^0| \Big[\left|\boldsymbol{\kappa}^0(\rho_j^-)\right|^2 + \left|\boldsymbol{\kappa}^0(\rho_{j-1}^+)\right|^2 \Big] + \frac{\lambda_1}{2h} \sum_{j=1}^{J} \left|\boldsymbol{h}_j^0\right|^2 \quad \textit{for all} \quad m > 0. \end{aligned}$$

Proof. The proof is similar to the proof of Theorem 5.2 below. □

5.2. Anisotropic case

Considering the problem (4.5)-(4.6), we adopt the backward Euler method in time, thus obtaining the following fully discretized problem: Given initial approximations $(\boldsymbol{x}^0, \boldsymbol{\kappa}_\gamma^0) \in [\mathbb{V}^h]^n \times [\mathbb{V}^h]^n$, find a discrete solution $(\boldsymbol{x}^m, \boldsymbol{\kappa}_\gamma^m) \in [\mathbb{V}^h]^n \times [\mathbb{V}^h]^n$ such that

$$\left(\frac{1}{\tau}\delta \boldsymbol{x}^m, \boldsymbol{\eta}^h\right)_{\Gamma^{m-1}} = \left(\gamma''(\boldsymbol{x}_s^{m-1})(\boldsymbol{\kappa}_\gamma^m)_s + \frac{1}{2}|\boldsymbol{\kappa}_\gamma^m|^2 \boldsymbol{x}_s^m - \lambda_2 \gamma(\boldsymbol{x}_\rho^m)\gamma'(\boldsymbol{x}_\rho^m), \boldsymbol{\eta}_s^h\right)_{\Gamma^{m-1}}, \tag{5.3}$$

$$\left(\delta \boldsymbol{\kappa}_\gamma^m, \boldsymbol{\xi}^h\right)_{\Gamma^{m-1}} = -\left(\gamma''(\boldsymbol{x}_s^{m-1})\delta \boldsymbol{x}_s^m, \boldsymbol{\xi}_s^h\right)_{\Gamma^{m-1}} - \left((\boldsymbol{x}_s^m \cdot \delta \boldsymbol{x}_s^m)\boldsymbol{\kappa}_\gamma^m, \boldsymbol{\xi}^h\right)_{\Gamma^{m-1}} \tag{5.4}$$

for all $(\boldsymbol{\eta}^h,\ \boldsymbol{\xi}^h) \in [\mathbb{V}^h]^n \times [\mathbb{V}^h]^n$ and $m > 0$, where $\delta \boldsymbol{x}^m := \boldsymbol{x}^m - \boldsymbol{x}^{m-1}$ and $\delta \boldsymbol{\kappa}_\gamma^m := \boldsymbol{\kappa}_\gamma^m - \boldsymbol{\kappa}_\gamma^{m-1}$.

Let $E_{\lambda_2}^m = E_\gamma^m + \lambda_2 D_\gamma^m$ be the discretized energy functional. Then the unconditional energy stability is established in the following theorem.

Theorem 5.2 (Energy Decay). *For $(\boldsymbol{x}^m, \boldsymbol{\kappa}_\gamma^m) \in [\mathbb{V}^h]^n \times [\mathbb{V}^h]^n$ with the initial curve Γ_0^h, the fully discretized problem* (5.3)-(5.4) *has the property*

$$\begin{aligned} & E_{\lambda_2}^m \le E_{\lambda_2}^{m-1} \le \cdots \le E_{\lambda_2}^0 \\ &= \frac{1}{4} \sum_{j=1}^{J} |\boldsymbol{h}_j^0| \Big[\left|\boldsymbol{\kappa}_\gamma^0(\rho_j^-)\right|^2 + \left|\boldsymbol{\kappa}_\gamma^0(\rho_{j-1}^+)\right|^2 \Big] \\ &\quad + \frac{\lambda_2 h}{4} \sum_{j=1}^{J} \Big[\gamma^2\big(\boldsymbol{x}_\rho^0(\rho_j^-)\big) + \gamma^2\big(\boldsymbol{x}_\rho^0(\rho_{j-1}^+)\big) \Big] \end{aligned}$$

valid for any $m > 0$.

Proof. Choosing $\boldsymbol{\eta}^h = \delta \boldsymbol{x}^m$, $\xi^h = \boldsymbol{\kappa}_\gamma^m$ in (5.3)-(5.4) and summing the equations obtained gives

$$\left(\frac{1}{\tau}\delta \boldsymbol{x}^m, \delta \boldsymbol{x}^m\right)_{\Gamma^{m-1}} + \left(\delta \boldsymbol{\kappa}_\gamma^m, \boldsymbol{\kappa}_\gamma^m\right)_{\Gamma^{m-1}} = -\left(\frac{1}{2}|\boldsymbol{\kappa}_\gamma^m|^2 \boldsymbol{x}_s^m - \lambda_2 \gamma(\boldsymbol{x}_\rho^m)\gamma'(\boldsymbol{x}_\rho^m), \delta \boldsymbol{x}_s^m\right)_{\Gamma^{m-1}}. \quad (5.5)$$

Taking into account the inequality

$$\|\boldsymbol{u}\cdot(\boldsymbol{u}-\boldsymbol{v})\| \geq \frac{1}{2}\|\boldsymbol{u}\|^2 - \frac{1}{2}\|\boldsymbol{v}\|^2,$$

we obtain

$$\begin{aligned}\left(\delta \boldsymbol{\kappa}_\gamma^m, \boldsymbol{\kappa}_\gamma^m\right)_{\Gamma^{m-1}} &= \left(\boldsymbol{\kappa}_\gamma^m - \boldsymbol{\kappa}_\gamma^{m-1}, \boldsymbol{\kappa}_\gamma^m\right)_{\Gamma^{m-1}} \\ &\geq \frac{1}{2}\left(\boldsymbol{\kappa}_\gamma^m, \boldsymbol{\kappa}_\gamma^m\right)_{\Gamma^{m-1}} - \frac{1}{2}\left(\boldsymbol{\kappa}_\gamma^{m-1}, \boldsymbol{\kappa}_\gamma^{m-1}\right)_{\Gamma^{m-1}} \\ &= \frac{1}{2}\left(\boldsymbol{\kappa}_\gamma^m, \boldsymbol{\kappa}_\gamma^m\right)_{\Gamma^{m-1}} - E_\gamma^{m-1}. \end{aligned} \quad (5.6)$$

Similar considerations show that

$$\begin{aligned}&\frac{1}{2}\left(|\boldsymbol{\kappa}_\gamma^m|^2 \boldsymbol{x}_s^m, \delta \boldsymbol{x}_s^m\right)_{\Gamma^{m-1}} \\ &\geq \frac{1}{4}\left(|\boldsymbol{\kappa}_\gamma^m|^2 \boldsymbol{x}_s^m, \boldsymbol{x}_s^m\right)_{\Gamma^{m-1}} - \frac{1}{4}\left(|\boldsymbol{\kappa}_\gamma^m|^2 \boldsymbol{x}_s^{m-1}, \boldsymbol{x}_s^{m-1}\right)_{\Gamma^{m-1}}, \end{aligned} \quad (5.7)$$

$$\begin{aligned}&\lambda_2\left(\gamma(\boldsymbol{x}_\rho^m)\gamma'(\boldsymbol{x}_\rho^m), \delta \boldsymbol{x}_s^m\right)_{\Gamma^{m-1}} \\ &= \lambda_2 \sum_{j=1}^J \left|\boldsymbol{h}_j^{m-1}\right| \left[\gamma(\boldsymbol{x}_\rho^m)\gamma'(\boldsymbol{x}_\rho^m) \cdot \frac{h}{|\boldsymbol{h}_j^{m-1}|}(\boldsymbol{x}_\rho^m - \boldsymbol{x}_\rho^{m-1})\right]\Big|_{I_j} \\ &\geq \lambda_2 \sum_{j=1}^J h\gamma\left(\boldsymbol{x}_\rho^m\right)\left(\gamma(\boldsymbol{x}_\rho^m) - \gamma(\boldsymbol{x}_\rho^{m-1})\right)\Big|_{I_j} \\ &\geq \lambda_2 \sum_{j=1}^J \frac{h}{2}\left(\gamma^2(\boldsymbol{x}_\rho^m) - \gamma^2(\boldsymbol{x}_\rho^{m-1})\right) = \lambda_2\left(D_\gamma^m - D_\gamma^{m-1}\right), \end{aligned} \quad (5.8)$$

where we used the convexity of γ. Furthermore, we note that

$$\begin{aligned}&\frac{1}{2}\left(\boldsymbol{\kappa}_\gamma^m, \boldsymbol{\kappa}_\gamma^m\right)_{\Gamma^{m-1}} + \frac{1}{4}\left(|\boldsymbol{\kappa}_\gamma^m|^2 \boldsymbol{x}_s^m, \boldsymbol{x}_s^m\right)_{\Gamma^{m-1}} - \frac{1}{4}\left(|\boldsymbol{\kappa}_\gamma^m|^2 \boldsymbol{x}_s^{m-1}, \boldsymbol{x}_s^{m-1}\right)_{\Gamma^{m-1}} \\ &= \frac{1}{4}\sum_{j=1}^J \left|\boldsymbol{h}_j^{m-1}\right| \left[|\boldsymbol{\kappa}_\gamma^m|^2(\rho_j^-) + |\boldsymbol{\kappa}_\gamma^m|^2(\rho_{j-1}^+)\right] \\ &\quad + \frac{1}{8}\sum_{j=1}^J \left|\boldsymbol{h}_j^{m-1}\right| \left[|\boldsymbol{\kappa}_\gamma^m|^2(\rho_j^-) + |\boldsymbol{\kappa}_\gamma^m|^2(\rho_{j-1}^+)\right] \frac{\boldsymbol{h}_j^m \cdot \boldsymbol{h}_j^m}{|\boldsymbol{h}_j^{m-1}|^2} \end{aligned}$$

$$
\begin{aligned}
&-\frac{1}{8}\sum_{j=1}^{J}\left|\boldsymbol{h}_j^{m-1}\right|\left[|\boldsymbol{\kappa}_\gamma^m|^2(\rho_j^-)+|\boldsymbol{\kappa}_\gamma^m|^2(\rho_{j-1}^+)\right]\frac{\boldsymbol{h}_j^{m-1}\cdot\boldsymbol{h}_j^{m-1}}{|\boldsymbol{h}_j^{m-1}|^2}\\
&=\sum_{j=1}^{J}\frac{|\boldsymbol{h}_j^{m-1}|+|\boldsymbol{h}_j^m|^2/|\boldsymbol{h}_j^{m-1}|}{8}\Big[|\boldsymbol{\kappa}_\gamma^m|^2(\rho_j^-)+|\boldsymbol{\kappa}_\gamma^m|^2(\rho_{j-1}^+)\Big]\\
&\geq\frac{|\boldsymbol{h}_j^m|}{4}\Big[|\boldsymbol{\kappa}_\gamma^m|^2(\rho_j^-)+|\boldsymbol{\kappa}_\gamma^m|^2(\rho_{j-1}^+)\Big]=E_\gamma^m. \qquad (5.9)
\end{aligned}
$$

Combining (5.5)-(5.9) gives

$$
E_{\lambda_2}^m-E_{\lambda_2}^{m-1}=\left(E_\gamma^m+\lambda_2 D_\gamma^m\right)-\left(E_\gamma^{m-1}+\lambda_2 D_\gamma^{m-1}\right)\leq-\left(\frac{1}{\tau}\delta\boldsymbol{x}^m,\delta\boldsymbol{x}^m\right)_{\Gamma^{m-1}}\leq 0,
$$

and the proof is complete. □

Remark 5.1. The approach used allows to construct an energy-stable method for classical elastic flows with appropriate tangential velocity. Recently, Deckelnick and Nürnberg [14] proposed a novel finite element scheme for curve diffusion and elastic flow in arbitrary codimension. They introduced explicit tangential velocity, so that the Dirichlet energy of the geometric flow decays. Consequently, a good mesh quality can be achieved. Nevertheless, there are still some problems that require further consideration.

5.3. BDF2 scheme

Starting with an initial solution $(\boldsymbol{x}^0,\boldsymbol{\kappa}_\gamma^0)\in[\mathbb{V}^h]^n\times[\mathbb{V}^h]^n$, we adopt the second-order BDF method to approximate the problem (4.5)-(4.6) of the modified anisotropic elastic flow in time direction, thus arriving at the following algorithm.

Step I. Find $(\boldsymbol{x}^1,\boldsymbol{\kappa}_\gamma^1)\in[\mathbb{V}^h]^n\times[\mathbb{V}^h]^n$ by solving the algebraic systems (5.3)-(5.4).

Step II. For $2\leq m\leq N$, find discrete solutions $(\boldsymbol{x}^m,\boldsymbol{\kappa}_\gamma^m)\in[\mathbb{V}^h]^n\times[\mathbb{V}^h]^n$ such that

$$
\left(\frac{1}{\tau}D_2\boldsymbol{x}^m,\boldsymbol{\eta}^h\right)_{\hat{\Gamma}^m}=\left(\gamma''(\hat{\boldsymbol{x}}_s^m)(\boldsymbol{\kappa}_\gamma^m)_s+\frac{1}{2}|\boldsymbol{\kappa}_\gamma^m|^2\boldsymbol{x}_s^m-\lambda_2\gamma(\boldsymbol{x}_\rho^m)\gamma'(\boldsymbol{x}_\rho^m),\boldsymbol{\eta}_s^h\right)_{\hat{\Gamma}^m}, \qquad (5.10)
$$

$$
\left(D_2\boldsymbol{\kappa}_\gamma^m,\boldsymbol{\xi}^h\right)_{\hat{\Gamma}^m}=-\left(\gamma''(\hat{\boldsymbol{x}}_s^m)D_2\boldsymbol{x}_s^m,\boldsymbol{\xi}_s^h\right)_{\hat{\Gamma}^m}-\left((\boldsymbol{x}_s^m\cdot D_2\boldsymbol{x}_s^m)\boldsymbol{\kappa}_\gamma^m,\boldsymbol{\xi}^h\right)_{\hat{\Gamma}^m} \qquad (5.11)
$$

for all $(\boldsymbol{\eta}^h,\ \boldsymbol{\xi}^h)\in[\mathbb{V}^h]^n\times[\mathbb{V}^h]^n$, where

$$
D_2\boldsymbol{f}^m:=\frac{3}{2}\boldsymbol{f}^m-2\boldsymbol{f}^{m-1}+\frac{1}{2}\boldsymbol{f}^{m-2},\quad \hat{\boldsymbol{g}}^m=2\boldsymbol{g}^{m-1}-\boldsymbol{g}^{m-2},
$$

and $\hat{\Gamma}^m$ is the polygonal curve parameterized by $\hat{\boldsymbol{x}}^m$.

Remark 5.2. Though we have not established the energy stability of the BDF2 scheme (5.10)-(5.11), our numerical examples in the following section suggest that the energy is consistently decreasing.

6. Numerical Examples

In this section, we present several examples to test the effectiveness, good mesh property, and unconditional energy stability of the proposed schemes. In order to determine $(\boldsymbol{x}^m, \boldsymbol{\kappa}_\gamma^m)$ in nonlinear systems (5.3)-(5.4), we use the following Newton-Raphson method: Given $(\boldsymbol{x}^{m,l}, \boldsymbol{\kappa}_\gamma^{m,l})$, $m > 0$ in the l-th iterative step and the initial value $(\boldsymbol{x}^{m,0}, \boldsymbol{\kappa}_\gamma^{m,0}) = (\boldsymbol{x}^{m-1}, \boldsymbol{\kappa}_\gamma^{m-1})$, find $(\boldsymbol{x}^{m,l+1}, \boldsymbol{\kappa}_\gamma^{m,l+1})$ such that the relations

$$
\begin{aligned}
&\frac{1}{\tau}\left(\boldsymbol{x}^{m,l+1}-\boldsymbol{x}^{m-1}, \boldsymbol{\eta}^h\right)_{\Gamma^{m-1}} \\
&= \Big(\gamma''(\boldsymbol{x}_s^{m-1})(\boldsymbol{\kappa}_\gamma^{m,l+1})_s + \boldsymbol{\kappa}_\gamma^{m,l}\cdot(\boldsymbol{\kappa}_\gamma^{m,l+1}-\boldsymbol{\kappa}_\gamma^{m,l})\boldsymbol{x}_s^{m,l}, \boldsymbol{\eta}_s^h\Big)_{\Gamma^{m-1}} \\
&\quad + \left(\frac{1}{2}|\boldsymbol{\kappa}_\gamma^{m,l}|^2\boldsymbol{x}_s^{m,l+1} - \lambda_2\big(\gamma'(\boldsymbol{x}_\rho^{m,l})\cdot\boldsymbol{x}_\rho^{m,l+1}\big)\gamma'(\boldsymbol{x}_\rho^{m,l}), \boldsymbol{\eta}_s^h\right)_{\Gamma^{m-1}} \\
&\quad - \Big(\lambda_2\gamma(\boldsymbol{x}_\rho^{m,l})\gamma''(\boldsymbol{x}_\rho^{m,l})\boldsymbol{x}_\rho^{m,l+1}, \boldsymbol{\eta}_s^h\Big)_{\Gamma^{m-1}}, \\
&\Big(\boldsymbol{\kappa}_\gamma^{m,l+1}-\boldsymbol{\kappa}_\gamma^{m-1}, \xi^h\Big)_{\Gamma^{m-1}} \\
&= -\Big(\gamma''(\boldsymbol{x}_s^{m-1})(\boldsymbol{x}_s^{m,l+1}-\boldsymbol{x}_s^{m-1}), \xi_s^h\Big)_{\Gamma^{m-1}} \\
&\quad - \Big(\big((2\boldsymbol{x}_s^{m,l}-\boldsymbol{x}_s^{m-1})\cdot(\boldsymbol{x}_s^{m,l+1}-\boldsymbol{x}_s^{m,l})\big)\boldsymbol{\kappa}_\gamma^{m,l}, \xi^h\Big)_{\Gamma^{m-1}} \\
&\quad - \Big(\big(\boldsymbol{x}_s^{m,l}\cdot(\boldsymbol{x}_s^{m,l}-\boldsymbol{x}_s^{m-1})\big)\boldsymbol{\kappa}_\gamma^{m,l+1}, \xi^h\Big)_{\Gamma^{m-1}}
\end{aligned}
$$

are valid for all $(\boldsymbol{\eta}^h, \xi^h) \in [\mathbb{V}^h]^n \times [\mathbb{V}^h]^n$.

We set the tolerance $\mathrm{tol} = 10^{-10}$ and use the following termination condition for the above iteration scheme:

$$
\max_{0\le j\le J}\Big(|\boldsymbol{x}^{m,l+1}(\rho_j)-\boldsymbol{x}^{m,l}(\rho_j)| + |\boldsymbol{\kappa}_\gamma^{m,l+1}(\rho_j)-\boldsymbol{\kappa}_\gamma^{m,l}(\rho_j)|\Big) \le \mathrm{tol}.
$$

Note that for the isotropic elastic flow (5.1)-(5.2) and BDF2 scheme (5.10)-(5.11) a similar iterative method is used. Testing the mesh quality over time evolution, we use the mesh ratio $\sigma(t)$ defined by

$$
\sigma(t) = \max_{1\le j\le J}|\boldsymbol{h}_j(t)| \,/\, \min_{1\le j\le J}|\boldsymbol{h}_j(t)|,
$$

in order to illustrate the asymptotic equidistribution of vertices. Moreover, we always choose a smooth initial curve Γ_0 with parameterization $\boldsymbol{x}^0$, so that we can obtain the initial curvature vector $\boldsymbol{\kappa}_\gamma^0$ by using the definition (1.7).

The parameter λ influences both the length of the steady-state curve and the mesh quality of the discrete curve. We aim to balance a sufficiently small λ to prevent the curve from vanishing during evolution with good mesh quality. In numerical computations, an appropriate value is determined through extensive testing. The value of λ lies in $[0, 0.1]$.

6.1. Modified isotropic elastic flow

Certain numerical validations of the scheme for isotropic elastic flow are presented below.

Example 6.1. We first test the convergence rate of the energy-stable scheme (5.1)-(5.2) for an exact solution with $\lambda_1 = 0$ as

$$\boldsymbol{x}(\theta,t) = (1+2t)^{1/4}(\cos\theta, \sin\theta), \quad \boldsymbol{\kappa}(\theta,t) = -(1+2t)^{-1/4}(\cos\theta, \sin\theta).$$

For simplicity, we always use $\theta := 2\pi\rho \in [0, 2\pi]$ instead of $\rho \in \mathbb{I}$ to represent the parameterization of a curve. The numerical errors are calculated as

$$\mathscr{E}_{\boldsymbol{x}^m} = \max_{0\le m\le M} \|\boldsymbol{x}(t_m) - \boldsymbol{x}^m\|_{L^2}, \quad \mathscr{E}_{\boldsymbol{\kappa}^m} = \max_{0\le m\le M} \|\boldsymbol{\kappa}(t_m) - \boldsymbol{\kappa}^m\|_{L^2},$$

where $(\boldsymbol{x}(t_m), \boldsymbol{\kappa}(t_m))$ and $(\boldsymbol{x}^m, \boldsymbol{\kappa}^m)$ are exact and numerical solution, respectively.

Table 1 shows errors and convergence orders of numerical solutions. Note that for initial mesh size and time step $(h_0, \tau_0) = (2^{-4}, 0.04)$, and final times $T = 1$ and $T = 50$, linear finite elements provide the second-order convergence.

Table 1: Errors and convergence orders for numerical solution of an expanding circle until $T = 1$ and $T = 50$.

(h,τ)	$T=1$				$T=50$			
	$\mathscr{E}_{\boldsymbol{x}^m}$	Order	$\mathscr{E}_{\boldsymbol{\kappa}^m}$	Order	$\mathscr{E}_{\boldsymbol{x}^m}$	Order	$\mathscr{E}_{\boldsymbol{\kappa}^m}$	Order
(h_0, τ_0)	1.59e-3	-	7.58e-3	-	3.16e-2	-	7.60e-3	-
$(h_0/2, \tau_0/4)$	4.05e-4	1.97	1.91e-3	1.99	7.94e-3	1.99	1.91e-3	1.99
$(h_0/2^2, \tau_0/4^2)$	1.02e-4	1.99	4.77e-4	2.00	1.99e-3	2.00	4.49e-4	2.00
$(h_0/2^3, \tau_0/4^3)$	2.55e-5	2.00	1.19e-4	2.00	4.97e-4	2.00	1.20e-4	2.00
$(h_0/2^4, \tau_0/4^4)$	6.37e-6	2.00	2.99e-5	2.00	1.24e-4	2.00	3.00e-5	2.00

Example 6.2. To compare the mesh quality in original and modified elastic flows, we select the initial curve as $\boldsymbol{x}(\theta) = (3\cos\theta, \sin\theta), \theta \in [0, 2\pi]$. The simulation parameters are set as $\tilde{\lambda}_1 = \lambda_1 = 0.01, \tau = 0.001, h = 2^{-6}$, and $T = 9$. Figs. 1-2 show that the classical elastic

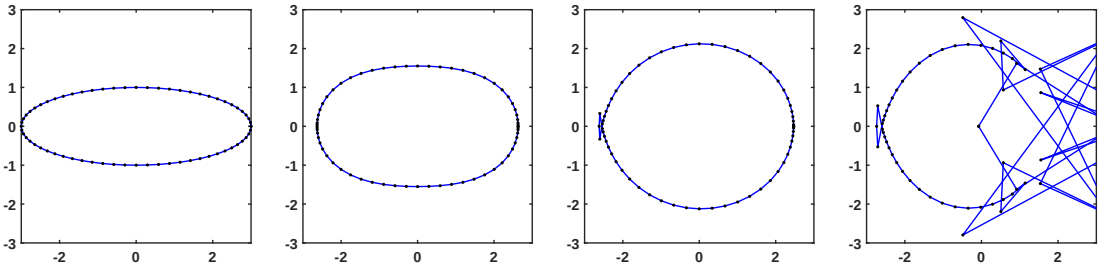

Figure 1: Snapshots of an ellipse evolving under the classical isotropic elastic flow at $t = 0, 3, 7, 9$.

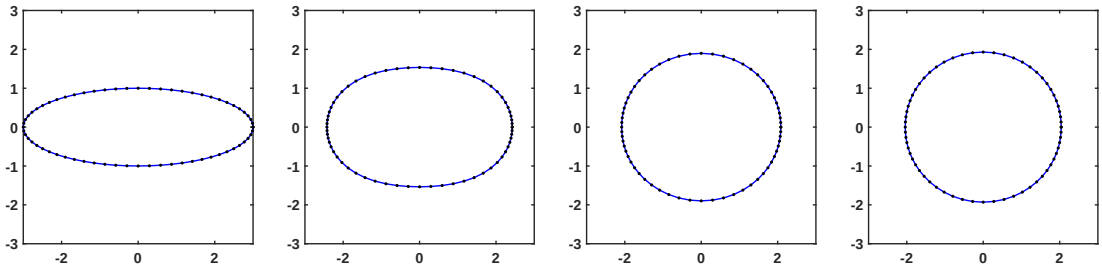

Figure 2: Snapshots of an ellipse evolving under the modified isotropic elastic flow at $t = 0, 3, 7, 9$.

flow causes mesh distortion, whereas the modified formulation asymptotically preserves mesh quality through uniform nodal distribution.

Example 6.3. Next, the numerical solution of a hypocycloid in $\mathbb{R}^2$ evolving under the modified isotropic elastic flow with $\lambda_1 = 0.002$ is considered. The initial parameterization is

$$\boldsymbol{x}(\theta) = \left(-\frac{5}{2}\cos\theta + 4\cos 5\theta, -\frac{5}{2}\sin\theta + 4\sin 5\theta\right), \quad \theta \in [0, 2\pi].$$

Given computational data $h = 2^{-7}$ and $\tau = 0.1$, Figs. 3(a)-3(d) demonstrate the snapshots of the evolving curve at $t = 0, 200, 650, 1500$. Note that 5 coverings of circle are stationary solutions, consistent with results [29]. Fig. 3(e) shows that the mesh ratio initially increases

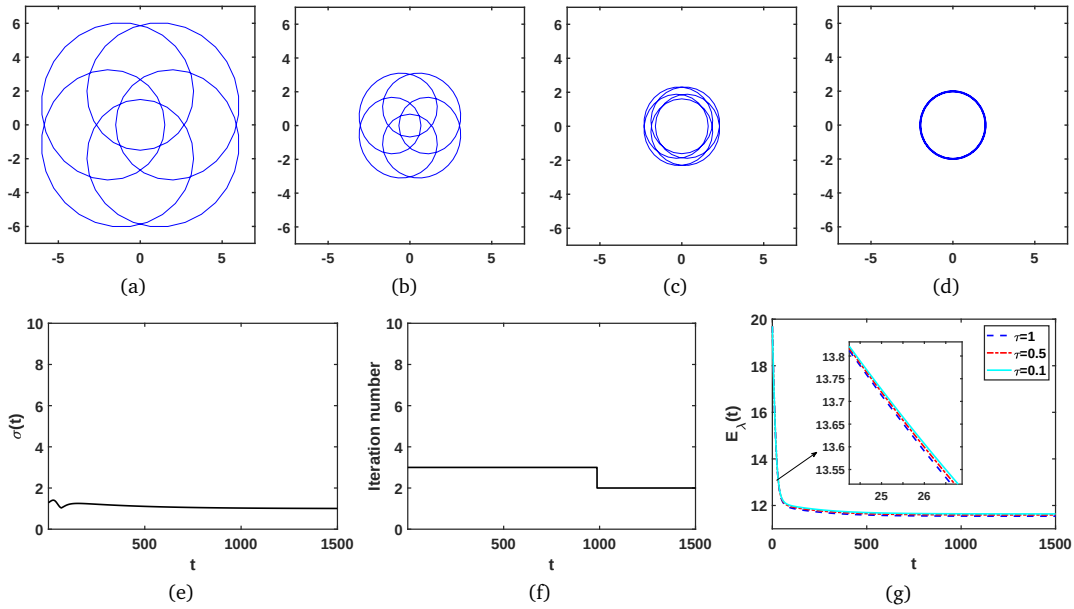

Figure 3: (a)-(d): Snapshots of the planar hypocycloid evolving under the modified isotropic elastic flow, (e)-(g): time histories of the mesh ratio $\sigma(t)$, the iteration number and the elastic energy $E_\lambda(t)$ with various time steps.

and then approximates 1 during evolution. Fig. 3(f) demonstrates the efficiency of the proposed iterative scheme, since fewer iterations are required. Moreover, for a fixed mesh size $h = 2^{-5}$, we note that the energy stability still holds for relatively large time steps in Fig. 3(g).

Example 6.4. Consider a torus knot in $\mathbb{R}^3$ evolving under modified isotropic elastic flow with $\lambda_1 = 0.005$ and

$$\boldsymbol{x}(\theta) = \big((3+\cos 15\theta)\cos\theta, (3+\cos 15\theta)\sin\theta, \sin 15\theta\big), \quad \theta \in [0, 2\pi].$$

Computational parameters are chosen as $h = 2^{-8}$, $\tau = 0.01$, and $T = 500$. The snapshots of evolving curve are plotted in Fig. 4. We observe that the initial torus knot eventually evolves into a stationary circle. The vertices tend to equally distribute during time evolution and oscillation occurs when the mesh experiences significant deformation, as shown in the left figure of Fig. 5. The number of iterations is presented in the middle. Furthermore, we examine the energy dissipation using different time steps $\tau = 0.5, 0.1, 0.01$ and a fixed mesh size $h = 2^{-5}$ in the right figure.

Example 6.5. Consider the evolution of a hypocycloid in $\mathbb{R}^3$ parameterized as follows:

$$\boldsymbol{x}(\theta) = \left(-\frac{5}{2}\cos\theta + 4\cos 5\theta, -\frac{5}{2}\sin\theta + 4\sin 5\theta, 0.5\sin 3\theta\right), \quad \theta \in [0, 2\pi].$$

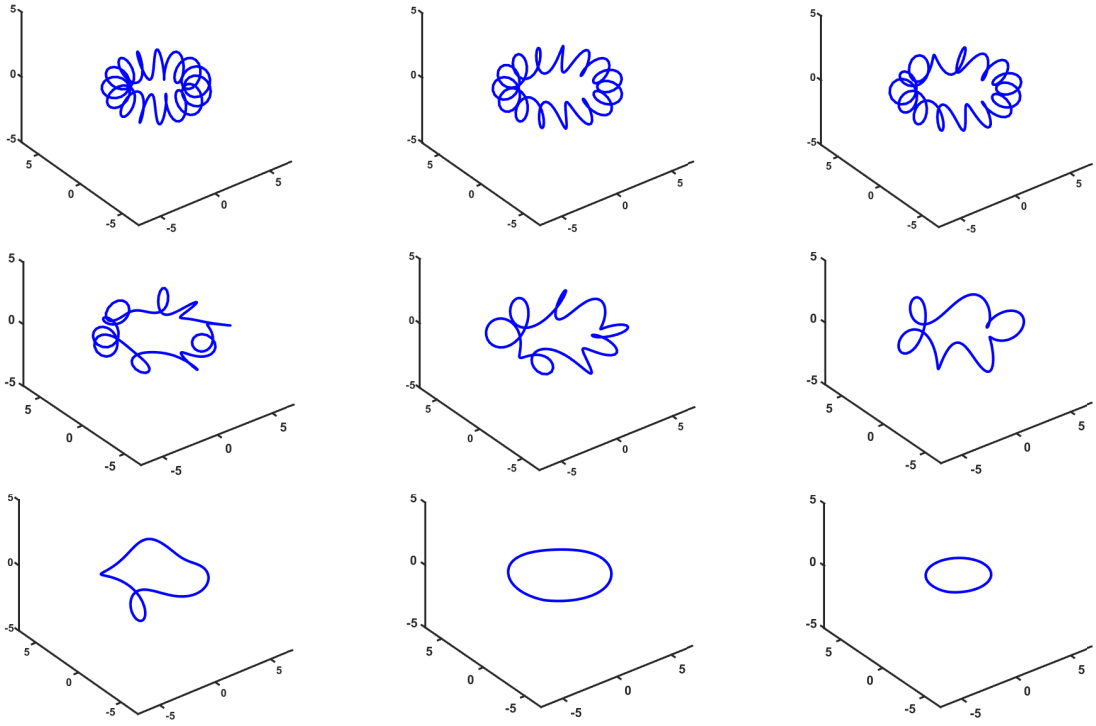

Figure 4: Snapshots of a torus knot evolving under the modified isotropic elastic flow at $t = 0$, $100, 105, 120, 125, 130, 135, 140, 500$.

The results of long time simulations with $\lambda_1 = 0.0025, h = 2^{-7}, \tau = 0.05$ and $T = 1000$ are shown in Fig. 6. Note that the curve gradually converges to a circle. The corresponding time history of the mesh ratio and iteration number are presented in Fig. 7, along with the modified elastic energy for a fixed mesh size $h = 2^{-5}$ and time steps $\tau = 1, 0.5, 0.1$.

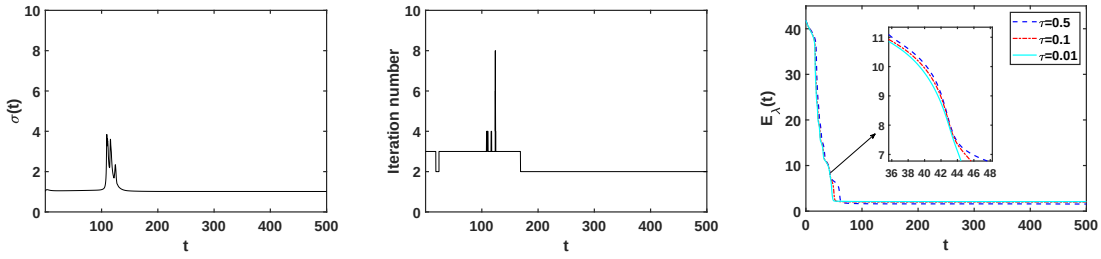

Figure 5: Torus knot in $\mathbb{R}^3$. Left: Time history of mesh ratio $\sigma(t)$. Middle: Iteration number. Right: Modified elastic energy $E_\lambda(t)$.

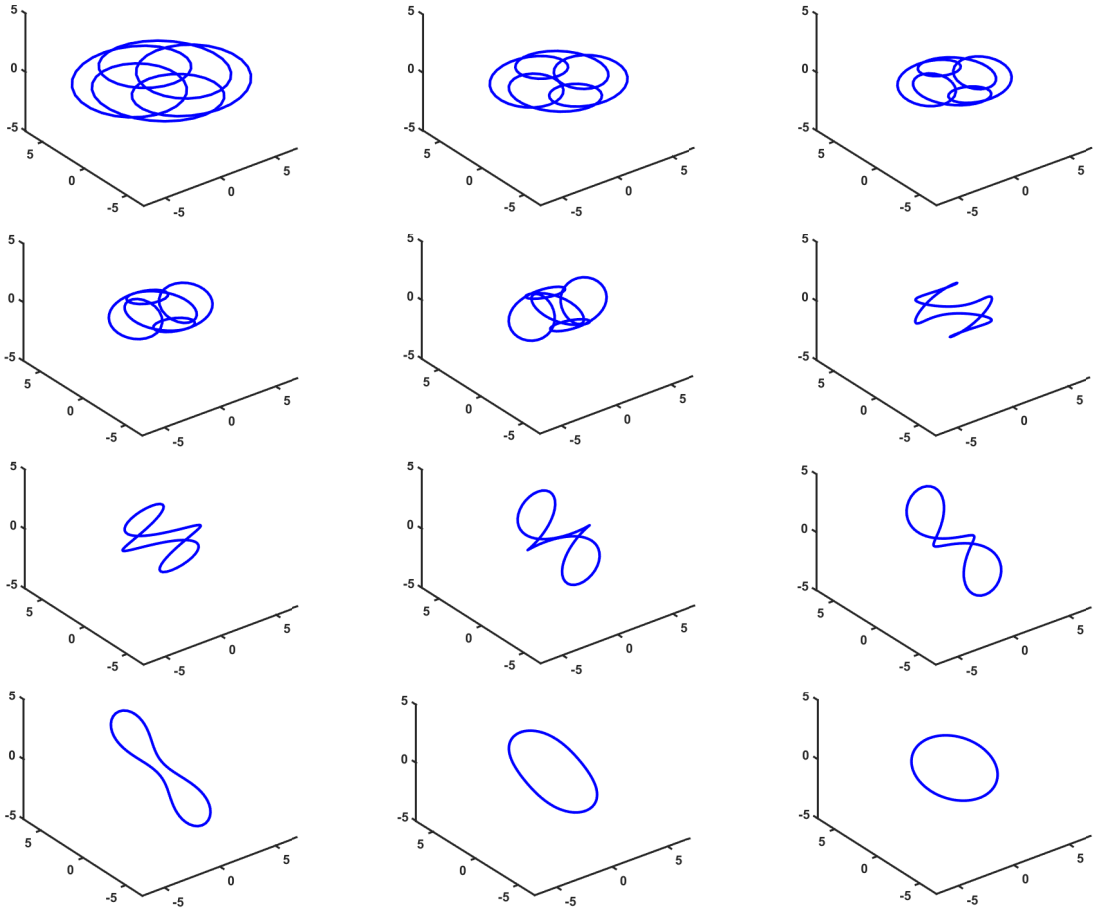

Figure 6: Snapshots of a hypocycloid in $\mathbb{R}^3$ evolving under the modified anisotropic elastic flow at $t = 0, 25, 50, 75, 100, 125, 150, 250, 300, 325, 350, 1000$.

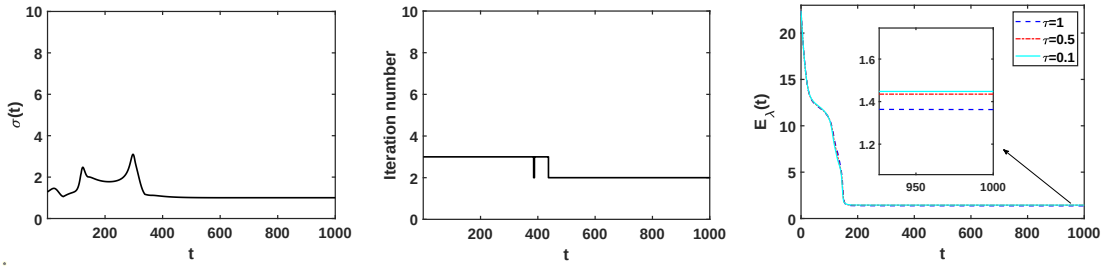

Figure 7: Hypocycloid in $\mathbb{R}^3$: Time history. Left: Mesh ratio $\sigma(t)$. Middle: Iteration number. Right: Elastic energy $E_\lambda(t)$.

6.2. Modified anisotropic elastic flow

Numerical examples of the new scheme for the modified anisotropic elastic flow are shown below.

Example 6.6. To observe anisotropic effects, we use the same initial setting as in the isotropic case. Then initial curve is an ellipse with the major-minor axis ratio 2. Besides, $\lambda_2 = 0.03, h = 2^{-6}, \tau = 10^{-4}$ and $T = 10$. We consider the L-fold, $\in \mathbb{N}^+$ anisotropic function

$$\gamma(\boldsymbol{p}) = \sum_{l=1}^{L} \sqrt{\left[\left(Q\left(\frac{2\pi}{L}\right)\right)^l\right]^T D(\varepsilon)\left(Q\left(\frac{2\pi}{L}\right)\right)^l \boldsymbol{p}\cdot\boldsymbol{p}}, \quad \varepsilon \in \mathbb{R}^+$$

with the rotation matrix

$$Q(\theta) = \begin{pmatrix} \cos\theta & \sin\theta \\ -\sin\theta & \cos\theta \end{pmatrix}$$

and the diagonal matrix $D = \mathrm{diag}\,(1, \varepsilon^2)$.

Fig. 8(a) shows the evolution under the modified isotropic elastic flow, while Figs. 8(b) and 8(c) display modified anisotropic cases with the parameters $(L, \varepsilon) = (2, 0.2)$ and $(L, \varepsilon) = (3, 0.1)$, respectively. The same initial curve thus evolves into three distinct shapes — viz. a circle (isotropic), a square ($L = 2$), and a hexagon ($L = 3$). The mesh ratio, the iterative number and the elastic energy are shown in Figs. 8(d)-8(f).

Example 6.7. The initial curve is a trefoil knot in $\mathbb{R}^3$ parameterized as

$$\boldsymbol{x}(\theta) = \big((2+\cos 3\theta)\cos 2\theta, (2+\cos 3\theta)\sin 2\theta, \sin 3\theta\big).$$

The results of simulation with the anisotropic function

$$\gamma(\boldsymbol{p}) = \sqrt{p_1^2 + 0.25(p_2^2 + p_3^2)}$$

are displayed in Figs. 9(a)-9(c). The parameters are $\lambda_2 = 0.01, h = 2^{-7}$, $\tau = 0.01$. Additionally, Figs. 9(e)-9(g) show the mesh ratio, iteration number and anisotropic elastic energy.

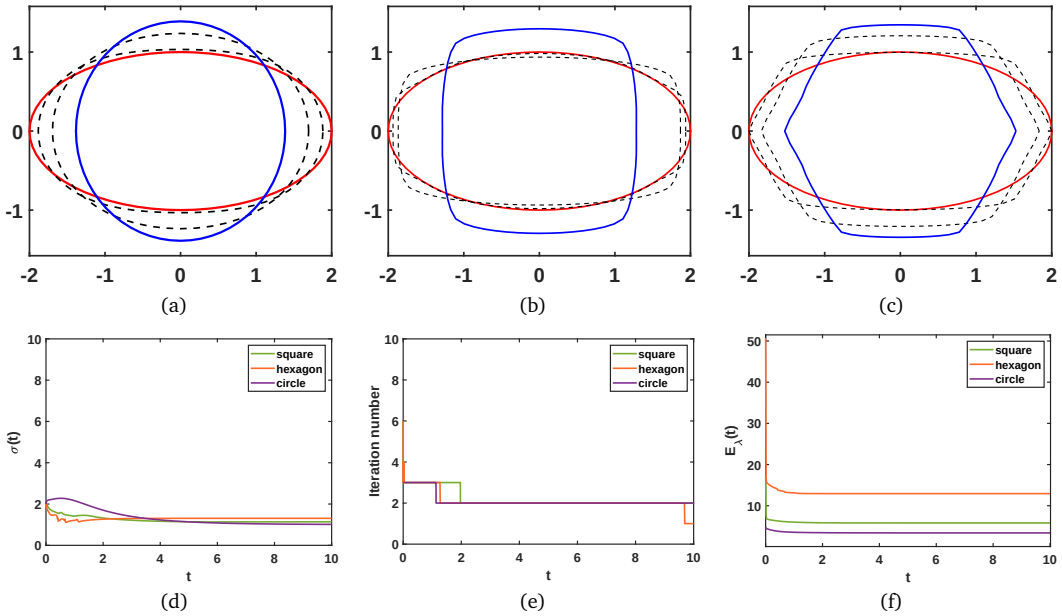

Figure 8: (a)-(c): Snapshots of an ellipse evolving into circle, square and hexagon under the modified anisotropic elastic flow. (d)-(f): Time history of mesh ratio $\sigma(t)$, iteration number and elastic energy $E_\lambda(t)$.

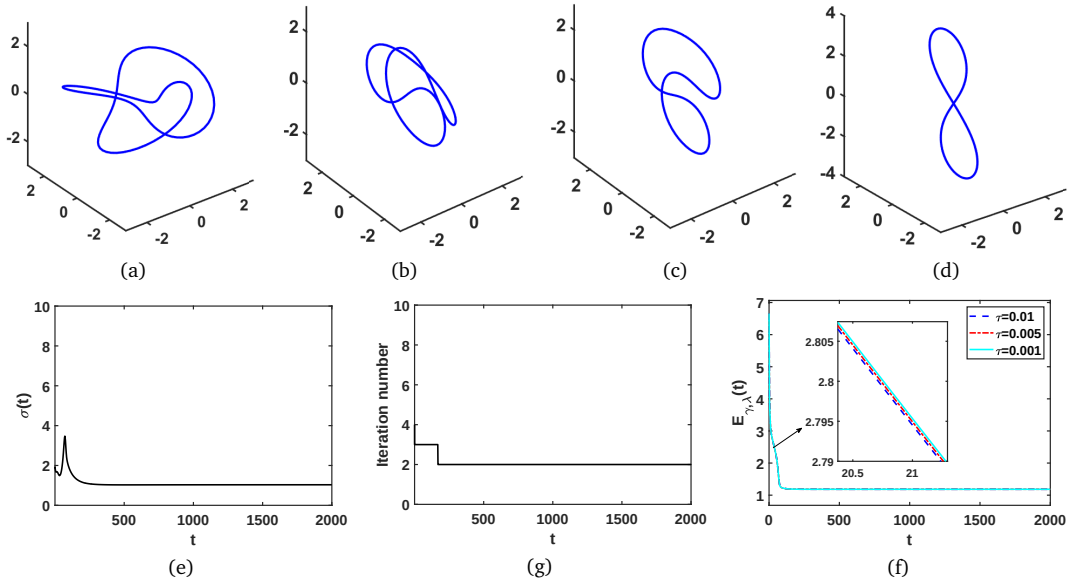

Figure 9: (a)-(d): Snapshots of trefoil knot evolving under modified anisotropic elastic flow. (e)-(g): Time history of mesh ratio $\sigma(t)$, iteration number and elastic energy $E_{\lambda,\gamma}(t)$ with various time steps.

6.3. BDF2 scheme

Example 6.8. To examine the convergence order of BDF2 scheme, we use the manifold distance

$$M(\Gamma,\Gamma') := |(\Omega\backslash\Omega')\cup(\Omega'\backslash\Omega)| = 2|\Omega\cup\Omega'| - |\Omega| - |\Omega'|,$$

where Ω and Ω' denote the regions enclosed by planar curves Γ and Γ', respectively, and $|\cdot|$ is the area of the corresponding region— cf. [38]. To measure the errors of numerical schemes with tangential motion, the manifold distance is more appropriate than the classical function metrics [23]. The error is calculated as

$$\mathscr{E}_{h,\tau}(t_m) = M\left(\boldsymbol{x}^m_{h,\tau}, \boldsymbol{x}^m_{h/2,\tau/2}\right).$$

We consider a lemniscate in $\mathbb{R}^2$ evolving under the modified anisotropic elastic flow with $\gamma = \sqrt{4q_1^2+q_2^2}$, $\lambda_2 = 0.01$. The initial parameters are $h_0 = 2^{-4}$ and $\tau_0 = 0.002$. Fig. 10 shows the second-order convergence in the time direction until $T = 1$ and 10 and the energy monotonic decay for different time steps until $T = 10$, along with snapshots of the evolution until $T = 100$.

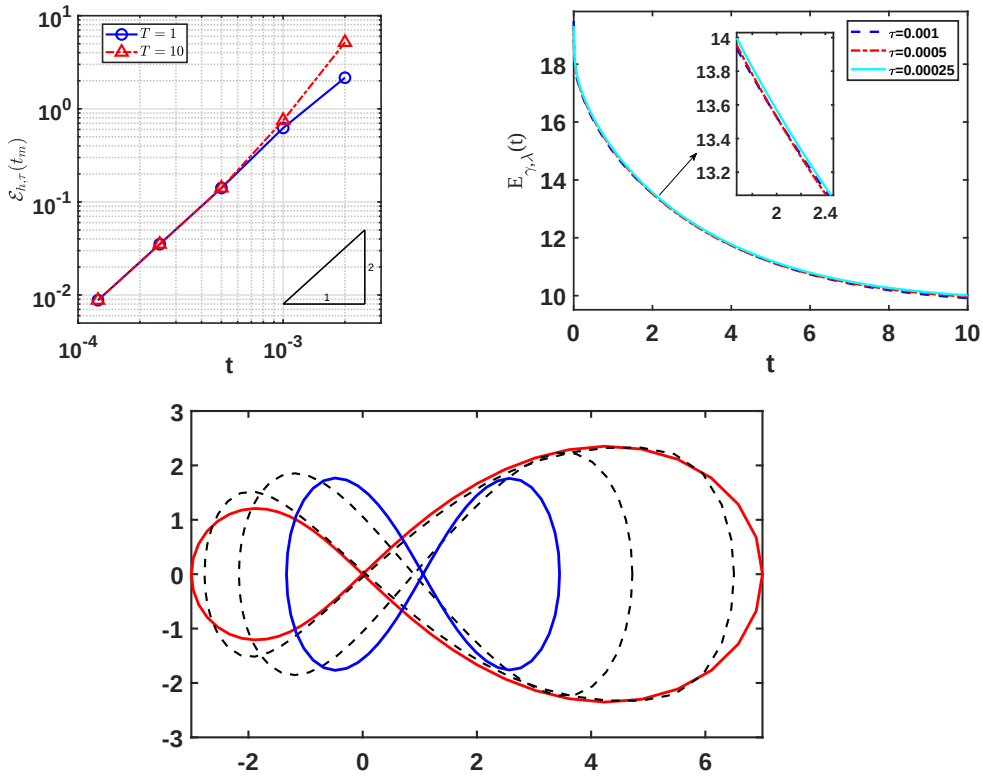

Figure 10: Left: Convergence order in time direction. Right: Time history of elastic energy. Bottom: Snapshots of a lemniscate in $\mathbb{R}^2$ evolving under modified anisotropic elastic flow.

7. Conclusions

In this paper, we propose new parametric finite element schemes for modified isotropic and anisotropic elastic flows of closed curves in $\mathbb{R}^n$. The new approach is energy-stable with improved mesh quality. First, we derive evolution equations for the parameterization and curvature vector of a curve and present the corresponding weak formulations. After that, a parametric finite element method is adopted to discretize weak formulations in space. It is proven that the semi-discretization is energy-stable. In addition, the backward Euler method and second-order BDF method are used to discretize the spatial semi-discrete scheme in the time direction. The proof of the energy decay property for the backward Euler method was provided in detail. Numerical examples using various curves in $\mathbb{R}^2$ and $\mathbb{R}^3$, show the efficiency method and unconditional energy stability of the full discretization.

The method proposed has asymptotic equal mesh distribution, due to the minimization of Dirichlet energy instead of the length functional. The corresponding energy-stable scheme for the classical elastic flow does not have good mesh quality. This problem will be addressed in the future. Computational extension of open curves is straightforward. However, the model itself requires well-posed boundary conditions to be physically meaningful. This aspect of the model's formulation remains a work for future research.

Acknowledgments

We thank the reviewers for their insightful comments and suggestions, which have significantly improved the quality of our manuscript.

This work is supported in parts by the National Natural Science Foundation of China (Grant Nos. 12361090, 1257011721), by the Natural Science Foundation of Xinjiang, China (Grant Nos. 2023D01C164, 2022D01D32), and by the Tianshan Talent Training Program (Grant Nos. 2022TSYCTD0019, 2023TSYCQNTJ0015).

References

[1] N. Adil, X.F. Xiao, K. Wang and X.L. Feng, *An ALE meshfree method for surface PDEs coupling with forced mean curvature flow*, J. Comput. Phys. **493**, 112467 (2023).

[2] W.Z. Bao, W. Jiang and Y.F. Li, *A symmetrized parametric finite element method for anisotropic surface diffusion of closed curves*, SIAM J. Numer. Anal. **61(2)**, 617–641 (2023).

[3] W.Z. Bao, W. Jiang, Y. Wang and Q. Zhao, *A parametric finite element method for solid-state dewetting problems with anisotropic surface energies*, J. Comput. Phys. **330**, 380–400 (2017).

[4] W.Z. Bao and Y.F. Li, *An energy-stable parametric finite element method for the planar Willmore flow*, SIAM J. Numer. Anal. **63(1)**, 103–121 (2025).

[5] J.W. Barrett, H. Garcke and R. Nürnberg, *Numerical approximation of gradient flows for closed curves in* $\mathbb{R}^d$, IMA J. Numer. Anal. **30(1)**, 4–60 (2010).

[6] J.W. Barrett, H. Garcke and R. Nürnberg, *Parametric approximation of isotropic and anisotropic elastic flow for closed and open curves*, Numer. Math. **120(3)**, 489–542 (2012).

[7] S. Bartels, *A simple scheme for the approximation of the elastic flow of inextensible curves*, IMA J. Numer. Anal. **33(4)**, 1115–1125 (2013).

[8] A. Bondarva, *Stability and error analysis for a numerical scheme to approximate elastic flow*, Ph.D. Thesis, Otto-von-Gueriche-Universität Magdeburg (2015).
[9] A. Bonito, R.H. Nochetto and M.S. Pauletti, *Parametric FEM for geometric biomembranes*, J. Comput. Phys. **229(9)**, 3171–3188 (2010).
[10] C. Bouchiat and M. Mezard, *Elastic rod model of a supercoiled DNA molecule*, Eur. Phys. J. E. **2**, 377–402 (2000).
[11] I. Chao et al., *A simple geometric model for elastic deformations*, ACM Trans. Graphics (TOG). **29(4)**, 1–6 (2010).
[12] A. Dall'Acqua, C.C. Lin and P. Pozzi, *Elastic flow of networks: Short-time existence result*, J. Evol. Equ. **21(2)**, 1299–1344 (2021).
[13] K. Deckelnick and G. Dziuk, *Error analysis for the elastic flow of parametrized curves*, Math. Comp. **78(266)**, 645–671 (2009).
[14] K. Deckelnick and R Nürnberg, *Finite element schemes with tangential motion for fourth order geometric curve evolutions in arbitrary codimension*, Numer. Math. **157**, 1313–1346 (2025).
[15] G. Dziuk, *Computational parametric Willmore flow*, Numer. Math. **111**, 55–80 (2008).
[16] G. Dziuk, E. Kuwert and R. Schatzle, *Evolution of elastic curves in $\mathbb{R}^n$: existence and computation*, SIAM J. Math. Anal. **33**, 1228–1245 (2002).
[17] B.P. Duan, *Energy-stable and mesh-preserving parametric FEM for mean curvature flow of surfaces*, SIAM J. Sci. Comput. **46(6)**, A3873–A3896 (2024).
[18] B.P. Duan and B.Y. Li, *New artificial tangential motions for parametric finite element approximation of surface evolution*, SIAM J. Sci. Comput. **46(1)**, A587–A608 (2024).
[19] C.M. Elliott and H. Fritz, *On approximations of the curve shortening flow and of the mean curvature flow based on the DeTurck trick*, IMA J. Numer. Anal. **37(2)**, 543–603 (2017).
[20] H. Garcke, J. Menzel and A. Pluda, *Long time existence of solutions to an elastic flow of networks*, Comm. Partial Differential Equations. **45(10)**, 1253–1305 (2020).
[21] H. Garcke, R. Nürnberg and Q. Zhao, *Stable fully discrete finite element methods with BGN tangential motion for Willmore flow of planar curves*, J. Sci. Comput. **105(2)**, 45 (2025).
[22] J.S. Hu and B.Y. Li, *Evolving finite element methods with an artificial tangential velocity for mean curvature flow and Willmore flow*, Numer. Math. **152**, 127–181 (2022).
[23] W. Jiang, C.M. Su and G.H. Zhang, *A second-order in time, BGN-based parametric finite element method for geometric flows of curves*, J. Comput. Phys. **514**, 113220 (2024).
[24] B. Kovács, B.Y. Li and C. Lubich, *A convergent evolving finite element algorithm for Willmore flow of closed surfaces*, Numer. Math. **149(3)**, 595–643 (2021).
[25] C.C. Lin, *L^2-flow of elastic curves with clamped boundary conditions*, J. Differential Equations. **252(12)**, 6414–6428 (2012).
[26] C.C. Lin and H.R. Schwetlick, *On the geometric flow of Kirchhoff elastic rods*, SIAM J. Appl. Math. **65(2)**, 720–736 (2004).
[27] Y.J. Liu, Y.Y. Qiao, X.F. Xiao and X.L. Feng, *Direct RBF-PU method combined with the tangent plane approach for parabolic equation on surface*, Eng. Anal. Bound. Elem. **165**, 105794 (2024).
[28] K. Mikula and D. Ševcovic, *Tangentially stabilized Lagrangian algorithm for elastic curve evolution driven by intrinsic Laplacian of curvature*, Proceedings of ALGORITMY **2005**, 1–10 (2005).
[29] A. Polden, *Curves and surfaces of least total curvature and fourth-order flows*, Ph.D. Thesis, Universität Tübingen (1996).
[30] M. Pozzetta, *Convergence of elastic flows of curves into manifolds*, Nonlinear Anal. **214**, 112581 (2022).
[31] P. Pozzi, *On an elastic flow for parametrized curves in $\mathbb{R}^n$ suitable for numerical purposes*, Ann. Mat. Pura Appl. (4). **202(5)**, 2541–2560 (2023).

[32] P. Pozzi and B. Stinner, *Elastic flow interacting with a lateral diffusion process: The one-dimensional graph case*, IMA J. Numer. Anal. **39(1)**, 201–234 (2019).
[33] P. Pozzi and B. Stinner, *Convergence of a scheme for an elastic flow with tangential mesh movement*, ESAIM-Math. Model. Num. **57(2)**, 445–466 (2023).
[34] R.E. Rusu, *An algorithm for the elastic flow of surfaces*, Interfaces Free Bound. **7(3)**, 229–239 (2005).
[35] Y. Wang, X.F. Xiao and X.L. Feng, *An accurate and parallel method with post-processing boundedness control for solving the anisotropic phase-field dendritic crystal growth model*, Commun. Nonlinear Sci. Numer. Simul. **115**, 106717 (2022).
[36] Y.Z. Wen, *Curve straightening flow deforms closed plane curves with nonzero rotation number to circles*, J. Differential Equations. **120(1)**, 89–107 (1995).
[37] G. Zhang, J. Li and Q.A. Huang, *A class of unconditionally energy stable relaxation schemes for gradient flows*, Math. Comput. Simulation. **218**, 235–247 (2024).
[38] Q. Zhao, W. Jiang and W.Z. Bao, *An energy-stable parametric finite element method for simulating solid-state dewetting*, IMA J. Numer. Anal. **41(3)**, 2026–2055 (2021).